

Millennium-length precipitation Reconstruction over South-eastern Asia: a Pseudo-Proxy Approach

Stefanie Talento^{1,2}, Lea Schneider¹, Johannes Werner, Jürg Luterbacher^{1,32}

1: Department of Geography, Climatology, Climate Dynamics and Climate Change, Justus-Liebig-University of Giessen, Germany

2: [Physics Institute, Science Faculty, Universidad de la República, Uruguay](#)

32: Center of International Development and Environmental Research, Justus Liebig University of Giessen, Giessen, Germany

Correspondence to: Stefanie Talento (stefanie.talento@geogr.uni-giessen.de)

Abstract

Quantifying [hydroclimateprecipitation](#) variability beyond the instrumental period is essential for putting current and future fluctuations into long-term perspective and to provide a test-bed for evaluating climate simulations. For South-eastern Asia such quantifications are scarce and millennium-long attempts are still missing. In this study we take a pseudo-proxy approach to evaluate the potential for generating summer precipitation reconstructions over South-eastern Asia during the past millennium. The ability of a series of novel Bayesian approaches to generate reconstructions at either annual or decadal resolutions and under diverse scenarios of pseudo-proxy records' noise is analysed and compared to the classic Analogue Method.

We find that for all the algorithms and resolutions a high-density of pseudo-proxy information is a necessary but not sufficient condition for a successful reconstruction. Among the selected algorithms, the Bayesian techniques perform generally better than the Analogue Method, being the difference in abilities highest over the semi-arid areas and in the decadal-resolution framework. The superiority of the Bayesian schemes indicates that directly modelling the space and time precipitation field variability ~~encapsulates more relevant value~~ [is more appropriate](#) than just relying in ~~similarities within a restricted~~ [a](#) pool of observational-~~based~~ analogues, in which certain [hydroclimateprecipitation](#) regimes might be absent. Using a pseudo-proxy network with locations and noise-levels similar to the ones found in the real world, we conclude that performing a millennium-long precipitation reconstruction over South-eastern Asia is feasible as the Bayesian schemes provide skilful results over most of the target area.

1. Introduction

Earth's climate varies in all spatial and temporal time-scales, as it is forced by either natural or

1 anthropic factors. To understand the dynamics of such variability, the analysis of the available
2 instrumental information is an essential tool. However, the time-coverage of the instrumental
3 records is rather short and, therefore, information from climate archives (natural and documentary)
4 going back centuries is important to put current and future changes into a long-term perspective and
5 to serve as a validation terrain for model simulations with the ultimate goal of understanding the
6 underlying physical mechanisms.

7

8 South-eastern Asian societies and economies are heavily dependent on the summer rainfall
9 (monsoon-dominated) as a fresh water resource, thus, it is important to investigate how these
10 precipitation patterns have varied in the past to provide a useful guide for the climate response to
11 future changes. Previous hydro Climate Field Reconstructions (CFRs) over Asia revealed a
12 substantial mismatch between modelled and reconstructed precipitation patterns (Shi et al. 2017)
13 and the spatial variability of large-scale droughts during the Little Ice Age (Cook et al. 2010, Feng
14 et al. 2013). While these studies covered the last 500-700 years, a gridded hydroclimate product
15 going beyond Medieval times on a spatio-temporal high resolution is yet missing. Whether such a
16 long and highly resolved reconstruction is possible given nowadays available data and
17 methodologies is the subject of this paper.

18

19 Reconstructing the temporal evolution of climatic variables in the space domain (~~Climate Field~~
20 ~~Reconstructions~~, CFR) based on the information from a sparse network of proxies and partially
21 overlapping instrumental data is a complex mathematical problem. First of all, the proxy data used
22 for generating reconstructions display a set of characteristics that make their use challenging: Their
23 distribution in space and time is heterogeneous with ~~decreasing numbers back in time~~ fewer records
24 further back in time; ~~most archives vary with respect to their temporal resolutions~~ different proxy
25 archives have different temporal resolutions and possibly including dating uncertainties; proxy
26 data might reflect different climate variables (temperature, precipitation, sea-level changes, pH, sea
27 water temperature, water mass circulation, etc.), recording climate conditions at different times of
28 the year, and this data contains non-climatic information (usually referred to as non-climatic noise).
29 Second, the overlap with instrumental observations is commonly short, limiting opportunities for
30 statistical learning and further validation. Third, and in contrast to average climate reconstructions,
31 CFR require the spatial scale-up of the available information therefore implying the need for
32 strategic inferring of the missing values in the target climate field, even in locations where no data
33 might be input. Finally, as the number of paleo climatic information becomes smaller back in time it
34 is virtually impossible to have an independent proxy data set to properly validate the output
35 reconstruction. A common approach to overcome this shortcoming and have a proper validation
36 stage is using a pseudo-reality. The process of using a Global Climate Model (GCM) simulation to
37 assess the ability of a reconstruction technique is known as Pseudo Proxy Experiment (PPE;
38 Smerdon, 2012; Mann and Rutherford, 2002). In a PPE, simulated data are modified to mimic real-
39 world proxies and instrumental observations (called pseudo-proxy and pseudo-instrumental data
40 sets) and the reconstruction algorithms are applied. The reconstruction results are then compared

1 with the available simulated target field, giving an estimation of the skill of the method in real-
2 world applications.

3

4 There are several ways to perform a CFR (see Luterbacher and Zorita, 2018 for a review). The
5 classical approach is through a multivariate regression perspective: a statistical relationship between
6 proxy and instrumental data is inferred from the overlapping (calibration) period and then, assuming
7 stationarity of this relationship, the missing instrumental values are predicted or reconstructed back
8 through time. Some of the most common techniques for climate reconstructions included in this
9 category are: Regularized Expectation-Maximization (RegEM, Schneider, 2001), Canonical
10 Correlation Analysis (CCA; Smerdon et al., 2010), Markov Random Fields (Guillot et al., 2015)
11 and the Analogue Method (Franke et al., 2011). The performance of these methods strongly depends
12 on the length of the instrumental data. If the overlapping period between proxy and instrumental
13 data is short, in comparison with the number of spatial locations considered, the estimation of the
14 covariance matrix is uncertain and the matrix inversion process is numerically unstable, leading to
15 poor performance when presented with new data out of the learning sample.

16

17 Another strategy to perform a CFR, more novel as it has only recently been applied in
18 paleoclimatology, is the Bayesian approach (e.g. Tingley and Huybers, 2010, 2013; Werner et al.,
19 2013; Luterbacher et al., 2016; Werner et al., 2018; Zhang et al., 2018). The Bayesian strategy is
20 probabilistic, incorporates information about the climate-proxy connection as constraints on the
21 reconstruction problem and has the benefit of providing more comprehensive uncertainty estimates
22 for the derived reconstructions. Robust comparisons between established methods and the emerging
23 efforts (Werner et al., 2013, Nilsen et al. 2018) underpin the benefits and justify further application
24 of the computationally more expensive method. So far, most of the paleoclimatic applications of
25 this methodology involve temperature reconstructions. Efforts to apply this probabilistic framework
26 to the more complex and highly variable hydroclimate are only in the initial stages, but the
27 advantages of the methodology over more classical approaches are auspicious.

28

29 Gómez-Navarro et al. (2015) used a pseudo-proxy experiment (PPE) approach to assess the skill of
30 several statistical techniques (classical regression methods and Bayesian) in reconstructing the
31 precipitation of the past two millennia over continental Europe. The authors find that none of the
32 schemes shows better performance than the others and that precipitation reconstructions over
33 Europe are only possible given a spatially dense and uniformly distributed network of proxies, as
34 the accuracy strongly deteriorates with distance to the proxy sites.

35

36 In this study we propose to evaluate, via PPE, the potential to generate a last-millennium summer
37 precipitation reconstruction for South-eastern Asia. We use ~~four~~ three CFR techniques: Bayesian
38 Hierarchical Modeling (BHM), BHM coupled with clustering processes (with two different
39 numbers of clusters) and Analogue Method. For each of the schemes we perform two

1 reconstructions: one at annual and one at decadal resolution. In addition, the influence of the noise
2 level in pseudo-proxies on the final reconstruction is evaluated.

3

4 This is the first time that a BHM approach is applied to the hydroclimate of Asia and its coupling
5 with clustering techniques is a methodological advance, conforming an innovation in the field. The
6 systematic evaluation of the skill of these probabilistic methods, and the comparison with the more
7 classical and well established Analogue technique, is a necessary step into learning about the
8 precipitation variability and the opportunities or obstacles to generate long-ranged informed guesses
9 about it. The PPE exercise is a fundamental validation step, essential for selecting the most
10 appropriate method to improve real-world reconstructions and, finally, derive a new and not
11 previously attempted gridded product of South-eastern Asia [summer](#) precipitation during the last
12 1000 years. [In this work only summer precipitation is targeted as the pseudo-proxy network
13 selected is based on real-world indicators of summer hydroclimatic variations \(see Data and
14 Methodology section\).](#)

15

16 The manuscript is organized as follows. In section 2 we present the data and methodology and
17 describe in detail the ~~threefour~~ reconstruction techniques, as well as the skill scores used for quality
18 evaluation. Section 3 is devoted to the results and discussions: we evaluate the skill of each of the
19 reconstruction methods, at both annual and decadal resolution, and investigate the role of the
20 pseudo-proxy noise. Finally, in section 4 we present conclusions and a short outlook.

21

22 2. Data and Methodology

23

24 2.1. Model

25

26 As a virtual reality setup for our study we use one full-forcing simulation (run 001) of the
27 Community Earth System Model (CESM) from the Last Millennium Ensemble (LME) Project
28 (Otto-Bliesner et al., 2016). The simulation is performed with horizontal resolution of $\sim 2^\circ$ ($\sim 1^\circ$) in
29 the atmosphere and land (ocean and ice) components. The CESM is forced with reconstructions of
30 the transient evolution of: solar intensity, volcanic emissions, greenhouse gases, aerosols, land use
31 conditions and orbital parameters, all together, for the period 850-2005. The target variable to
32 reconstruct is [June-July-August \(JJA\)](#) precipitation over continental Southeast Asia, here defined as
33 all continental grid points in the domain: Equator-50N, 72.5E-127.5E. Given the model resolution,
34 this implies that the reconstruction is attempted over 366 grid points.

35

36 Figure 1 depicts the JJA mean precipitation in the run used in this manuscript, considering only the
37 last 100 years of simulation (period 1906-2005). Historical simulations with the CESM show a

1 reasonable performance at reproducing summer precipitation over continental Asia: the simulated
2 JJA precipitation is generally in agreement with observations, although a false rainfall center over
3 the eastern Qinghai-Tibetan Plateau is generated in these simulations (Wang et al., 2015).

4

5 2.2. Proxy Data locations

6

7 For this study we select the locations of 47 real-world precipitation/drought sensitive proxies in the
8 target domain, that span the last millennium. The locations of tree ring, speleothem, lake sediment
9 and ice core sites as well as of some documentary data are mainly derived from the networks used
10 in Chen et al. (2015) and Ljungqvist et al. (2016) (Table 1). [The criteria for the selection of records](#)
11 [was: millennium-long \(with start date before 1000CE\), at least two values per century, terrestrial, published](#)
12 [in the peer-reviewed literature and described as indicator of local variations in hydroclimate.](#)

13 2.3. Design of the Pseudo Proxy Experiments (PPEs)

14

15 For the design of the PPE we build two data networks: a pseudo proxy and a pseudo instrumental.
16 The pseudo proxy network is based on the locations of the real-world hydroclimate proxies listed in
17 Table 1. As some of these 47 records are in close proximity, this translates into having 38 different
18 model grid points (about 10% of the total grid points in the study region). The selected locations are
19 not evenly distributed across South-eastern Asia: the highest concentrations are found over East
20 China and over the dry lands in the northwest of the study region (Fig. 1). There are neither pseudo
21 proxy sites southward of 20N, nor over Mongolia and the Himalayas. To emulate real proxies, we
22 consider the modelled precipitation time-series spanning the complete period of the simulation
23 (1156 years, either with annual or decadal resolution) at each of the 38 selected sites and
24 contaminate them by the addition of noise. We select four different levels of additive Gaussian
25 white noise, corresponding to null, low, medium, and high levels of noise. The selected noise levels
26 are such that the correlation between the original and the contaminated time-series is: 1, 0.7, 0.5 and
27 0.3, respectively. A correlation equal to 1 implies an idealised situation of perfect proxies to study
28 the representativeness of our spatial sampling. A correlation of 0.7 represents an optimistic
29 situation, but still realistic: for example, Shi et al. (2014) find correlations of up to 0.7 with a tree-
30 based reconstruction of the South Asian Summer Monsoon Index. A correlation of 0.5 between the
31 proxy series and precipitation corresponds to a medium-level noise, and could be regarded as the
32 average situation with real proxies (examples for Asia: He et al., 2018; Liu et al., 2013). A
33 correlation of 0.3 represents a high-noise setting, which is still rather common in real-world proxies
34 (e.g. Jones et al. 1999).

35

36 For the pseudo instrumental network we consider all the locations for which a reconstruction is
37 targeted: 366 model-grid points in South-eastern Asia. For each of these locations, we take the
38 modelled precipitation time-series for the last 100 years of simulation (at either annual or decadal

1 resolution) and add a small Gaussian-noise to represent the instrumental errors present in real
2 precipitation measurements. The added noise is such that, at each location, the correlation between
3 original and contaminated time-series is 0.95.

4

5 As an example, Figure 2 shows the simulated precipitation time-series at location [20N,82.5E] (east
6 India) together with the associated pseudo proxy and instrumental time-series, both at annual and
7 decadal resolution, for the case of medium-noise level (corresponding to a 0.5 correlation with the
8 target precipitation). At annual resolution, the simulated mean JJA precipitation at this site is 241
9 mm/month, with a standard deviation of 48 mm/month. ~~The time-series shows a weak drying trend~~
10 ~~(-0.8 mm/month per decade) and decrease in variance, although none of these changes are~~
11 ~~statistically significant. No statistically significant changes are found either in mean or variance.~~ The
12 maximum (minimum) summer precipitation at this location is 423 (87) mm/month and occurred in
13 the year 1022 (1208) of the simulation, respectively. At decadal resolution, the standard deviation is
14 reduced to 14 mm/month and the maximum (minimum) precipitation value is 283 (208) mm/month,
15 occurring at the period 1180-1189 (870-879).

16 2.4. Reconstruction Techniques

17

18 In the following subsections we describe in detail each of the ~~three~~four reconstruction techniques
19 used in this manuscript.

20 2.4.1. Bayesian Hierarchical Modelling (BHM)

21

22 In the BHM technique a hierarchy of parametric stochastic models is used to describe the
23 relationship between climate, instrumental and proxy data. The model parameters are estimated
24 using the available data, through the Bayes's rule. ~~The approach splits the complex relationship~~
25 ~~model into~~hierarchy consists of three basic components. First, in the process level, a stochastic
26 model describing the time evolution of the climate variable is selected. Second, in the data level,
27 stochastic relationships between the instrumental and proxy data and the climate variable are
28 developed. Finally, a level of prior information about the parameters involved in the other two
29 components of the hierarchy is coupled. Here we use the BHM algorithm named Bayesian
30 Algorithm for Reconstructing Climate Anomalies in Space and Time (BARCAST), developed by
31 Tingley and Huybers (2010). Following, we specify the assumptions and equations for each of the
32 levels in the model hierarchy.

33

34 **Process level:**

35 The process level describes the evolution of the true climatic field as a multivariate autoregressive
36 process of order 1, AR(1), with spatially correlated innovations.

1
2
3
4
5
6
7
8
9
10
11
12
13
14
15
16
17
18
19
20
21
22
23
24
25
26
27
28
29
30
31
32
33
34
35
36
37

The evolution of the true precipitation, sampled at a finite number of spatial locations, is assumed to follow a first-order autoregressive process:

$$Pr_{t+1} - \mu = \alpha (Pr_t - \mu) + \epsilon_{Pr,t} \quad (1)$$

where Pr_t is the vector consisting of the true precipitation values in all the locations at time step t , μ is the mean of the process, α the AR(1) coefficient. Note that the coefficients μ and α are the same for all the locations. To account for different precipitation means at each location the following procedure is followed: first, the time-series are standardized; second, the BHM is applied; finally, the outputs are inversely de-standardized. The standardization is performed using the sample mean and standard deviation from the pseudo instrumental times-series. The innovations $\epsilon_{Pr,t}$, accounting for the interannual or interdecadal variability, are assumed to be independent and identically distributed (iid) normal draws $\epsilon_{Pr,t} \sim N(0, \Sigma)$ with an exponentially-decaying spatial structure:

$$\Sigma_{ij} = \sigma^2 e^{-\phi |x_i - x_j|} \quad (2)$$

where $|x_i - x_j|$ is the distance between the locations i -th and j -th of the precipitation vector, ϕ is the range parameter (being $1/\phi$ the e-folding distance) and σ is the partial sill of the spatial covariance matrix (spatial persistence, homogeneous in space).

The temporal model within BARCAST allows the estimations of the field at a certain temporal step to be influenced by the information in the previous time-step. The assumed covariance matrix structure is supposed constant in time and follows an exponentially decaying pattern with distance. Note that, by assuming this structure if two distant locations have well-correlated precipitation time-series this will not be well represented by the BARCAST model assumed. The method parameterizes the spatial covariance matrix with two unknown parameters: the covariance at null distance (σ) and the exponential decay rate with distance (ϕ).

The model assumes that the climatic variable, precipitation, follows a Gaussian distribution. Although this might not be the case, especially for arid regions, the simulated JJA precipitation in the area of study can be taken to reasonably follow this assumption: for the pseudo-proxy selected locations 63% of the time-series (considering the instrumental period) pass the Kologorov-Smirnov test for normality at a 95% confidence level (Figure A1). Despite the Gaussian conditions are not met in all the grid points the model is still valid, although it might not be the most optimal fit at these locations.

Figure 3 shows the correlation decay with distance for the simulated JJA precipitation for different latitudinal bands. For annual data (Figure 3a), the correlation between precipitation time-series in

1 consecutive grid-points is usually high, around 0.8. With few exceptions, the simulated precipitation
 2 follows an exponentially-decaying pattern with distance, with points located further away than
 3 600km showing no significant correlation. Therefore, we take the exponentially-decaying spatial
 4 structure of the covariance matrix in BARCAST to be a reasonable assumption for the model. For
 5 decadal data (Figure 3b), the correlations behaviours are not uniform with respect to the latitudinal
 6 bands. ~~While~~ for some of the latitudes the plot follows an exponentially-decaying shape, for others
 7 it additionally evidences a teleconnection-pattern (notably the northern-most ~~and southern-most~~
 8 ~~latitude bands considered: 44N-48N latitude band and 10N-14N, respectively~~) ~~this assumption is~~
 9 ~~clearly flawed as it even evidences a teleconnection-pattern and not just a distance-decaying~~
 10 ~~behaviour.~~

11

12 **Data level:**

13 The data level specifies the relationship between the measurements (both proxy and instrumental)
 14 and the true field values.

15

16 The instrumental observations at each time are assumed to be noisy variations of the true
 17 precipitation field:

$$18 \quad Inst_t = H_{Inst,t} (Pr_t + \epsilon_{Inst,t}) \quad (3)$$

19

20 the noise terms are assumed to be iid multivariate normal draws $\epsilon_{Inst,t} \sim N(0, \tau_{Inst}^2)$, while

21 $H_{Inst,t}$ is a diagonal matrix with a one in position (i,i) if an instrumental observation is available
 22 at the i-th location, with a zero otherwise.

23

24 The proxy observations are assumed to follow an unknown statistically linear relationship with the
 25 true precipitation at each location:

$$26 \quad Proxy_t = H_{Proxy,t} (\beta_1 Proxy_t + \beta_0 + \epsilon_{Proxy,t}) \quad (4)$$

27

28 again, the $H_{Proxy,t}$ is a diagonal matrix with ones only for the locations with proxy observations,

29 and the noise terms are iid normal draws: $\epsilon_{Proxy,t} \sim N(0, \tau_{Proxy}^2)$

30

31 **Prior level:**

32 To close the scheme, prior distributions must be specified for the eight scalar parameters
 33 $(\alpha, \mu, \sigma, \phi, \beta_1, \beta_2, \tau_{Inst}^2, \tau_{Proxy}^2)$ and the initial climate field (i.e. at the first time-step). We follow the
 34 approach use the same priors as in Tingley and Huybers (2010) and select prior distributions that are
 35 sufficiently diffuse to not have any important influence on the posterior distributions.

36

1 Using Bayes' rule the posterior distribution of each of the unknown variables can be calculated.
2 Samples are drawn from this posterior distributions using a Gibbs sampler, with a Metropolis step
3 (Gelman et al, 2003) to update ϕ , the spatial range parameter. ~~Before applying the BHM all the~~
4 ~~proxy time-series are standardized using the sample mean and standard deviation from the pseudo~~
5 ~~instrumental times-series at the same locations.~~ The output of the Bayesian algorithm is not a
6 unique reconstruction, but an ensemble of 1200 equally-probable draws all of them consistent with
7 the model equations.

8 2.4.2. Bayesian Hierarchical Modelling coupled to Clustering

9
10 Here we propose to couple the BHM with a clustering algorithm. The aim of the clustering step is to
11 segregate South-eastern Asia into several clusters, according to similarities in the precipitation
12 regimes during the pseudo-instrumental period. After the clustering, the BHM code is run within
13 each cluster in an independently manner. Finally, all the results are merged together to produce the
14 entire spatial reconstruction over the post 850 period. The idea behind the clustering step is to
15 reduce the complexity of the problem to be presented to the BHM algorithm, as after clustering the
16 code does not have to deal with extreme differences in precipitation regimes (as dipole patterns at
17 mountain ranges) and large number of grid cells.

18

19 We use a hierarchical agglomerative clustering technique. Each observation starts in its own cluster
20 and pairs of clusters are agglomerated as one moves up in the hierarchy (Izenman, 2008). We select
21 a complete-linking strategy: the distance between sets of observations is defined as the maximum of
22 the pairwise distances between the observations in each of the sets. First, the method groups
23 together the two closest observations, according to the selected distance, creating a cluster of two
24 observations. Then, the sets whose distance is minimum are agglomerated together, iteratively
25 repeating the process.

26

27 Here, the elements to cluster together are the different grid-points in South-eastern Asia. The input
28 variables for the method are the pseudo-instrumental precipitation time-series at each of these
29 locations. The distance between two points is defined as: One minus the correlation between the
30 pseudo-instrumental precipitation time-series at these locations (points highly correlated display a
31 small distance). In this way, the method groups together points whose pseudo-instrumental
32 precipitation time-series are highly correlated. We should note that the clustering algorithm does not
33 require any expert-knowledge as it is a fully unsupervised machine learning technique. This
34 characteristic makes it easy to apply as a pre-BHM stage in any other context or area of study.

35

36 For both, the annual and the decadal, reconstructions we select two cases: clustering into 5 and into
37 10 groups (note that the clusters might be different when using the annual/decadal information, see
38 Figure A2). We term the reconstructions in this category: BHM+5Clusters and BHM+10Clusters.

The criteria for the selection of the number of clusters was that most of the clusters should include pseudo-proxy locations (if a cluster does not include pseudo-proxy information the BHM scheme only uses instrumental-period data). While this condition is met without problems for 5 Clusters, with the 10 Clusters division (at both annual and decadal cases) one of the clusters is disjunct with the pseudo-proxy network. As a consequence, a higher number of clustering divisions was not attempted.

2.4.3. Analogue Method

The Analogue Method is a learning technique first introduced by Lorenz (1969) for weather forecasting. The technique uses predictors to determine the value of the target variable, based on the statistical relationship between them in a learning set: the so-called pool of possible analogues. The method can also be applied to produce a CFR. In our study and for each time step (year or decade), the predictor variables are the proxy records (38 predictors) and the target variable is the complete precipitation field at the given time-step. For the annually-resolved reconstruction the learning set consists of the precipitation fields at each of the year-time-steps in the instrumental period, i.e. all the time-steps in which we simultaneously have the information about proxy and target. For the decadal-resolved reconstruction, the learning set consists of the mean precipitation field in each possible 10-years period during the instrumental era.

The reconstruction of the precipitation field at time-step t is obtained as follows. First, a distance between time-steps is defined. Let t_i be a time-step included in the pool (instrumental period). Then, the distance between t and t_i is, in this paper, defined as the Euclidean distance between the vectors of proxy data at times t and t_i :

$$d(t, t_i) = \sqrt{\sum_{j=1}^K (Prox(l_j, t) - Prox(l_j, t_i))^2} \quad (5)$$

where $Prox(l_j, t)$ is the value of the proxy at location l_j and time t . Locations l_1, \dots, l_K are all the proxy locations ($K=38$). Second, the time-steps in the pool are ordered according to their distance from t . Third, the N closest time-steps are selected from the pool, and termed analogues: t_1, \dots, t_N . Finally, the precipitation reconstruction for time t is the mean of the precipitation field in the N analogues:

$$Reconstruction(t) = \frac{Pr(t_1) + \dots + Pr(t_N)}{N} \quad (6)$$

N can be any value between 1 and the total number of elements in the pool of analogues time-steps in the instrumental period (100 for yearly reconstruction, 14 for decadal reconstruction). On the one hand, for annual (decadal) reconstructions using $N=1$ will imply having a reconstruction identical to just 1 year (10-years mean) of the instrumental period and, therefore, particularities of this year (10-years period) might be involved. On the other hand, using the maximal N implies just giving as

1 reconstruction the mean during the instrumental period, which eliminates all the inter-annual or
 2 inter-decadal variability. In this paper we select as N intermediate values, considering N
 3 approximately equal to 20% of the number of possible analogues time-steps in the instrumental
 4 period: 20 for the annual reconstruction, 2 for the decadal reconstruction. Experiments using values
 5 of N between 15% and 40% of the number of possible analogues were performed and the results are
 6 not significantly different as the ones selected to display here (not shown).

7

8 Note that in this manuscript we use the Analogue Method in its classical version (obtaining the pool
 9 of analogues from the observational data set) and not in combination with the use of an GCM to
 10 draw the Analogue cases from.

11

12 2.5. Skill Metrics

13

14 To evaluate the performance of the CFR methodologies we compare the reconstruction with the true
 15 precipitation field. We select three different skill metrics. The first skill metric, the Correlation
 16 Coefficient, evaluates the ability of the reconstruction to reproduce the temporal evolution of the
 17 target. At each grid point, we calculate the Pearson correlation between the reconstruction and the
 18 true precipitation time-series, considering the whole reconstruction period. As for the Bayesian
 19 algorithms we have an ensemble of reconstructions we first calculate the correlation of each of
 20 these ensembles with the true precipitation and, finally, we show the mean of these correlations.

21

22 The second skill metric quantifies the absolute biases of the reconstruction at each location. Instead
 23 of directly using the Root Mean Squared Error (RMSE), we compare the RMSE of the different
 24 reconstructions with the RMSE obtained with the simplest possible reconstruction: using the
 25 climatological mean during the instrumental period. In reconstruction studies, this is usually
 26 referred to as the Reduction of Error (RE, Cook et al., 1994) and is defined, at each location l, as:

$$27 \quad RE(l) = 1 - \frac{\sum_t (Pr(l,t) - Reconstruction(l,t))^2}{\sum_t (Pr(l,t) - Climatology(l))^2} \quad (7)$$

28

29 where $Reconstruction(l,t)$ is the reconstruction being evaluated at location l and time-step t and
 30 $Climatology(l)$ is the climatological mean at location l. The sum is done over all the time-steps
 31 within the reconstruction period. In this case for the Bayesian techniques, and to simplify the
 32 interpretation, we show this metric for the median reconstruction.

33

34 The last skill metric is especially designed to evaluate probabilistic ensemble forecasts of
 35 continuous predictands and is, therefore, particularly suitable for evaluating the Bayesian schemes.

1 We use the Continuous Ranked Probability Score (Hersbach 2000; Wilks, 2011; Werner et al.,
2 2018). The CRPS measures the difference between the accumulated probability density function
3 and the step function that jumps from 0 to 1 at the observed value:

$$4 \quad CRPS = \int_{-\infty}^{\infty} (F(y) - F_0(y))^2 dy \quad (8)$$

$$5 \quad F_0(y) = \begin{cases} 0, & y < \text{observed value} \\ 1, & y \geq \text{observed value} \end{cases} \quad (9)$$

6 It has a negative orientation, meaning smaller values are better. This metric can only be provided
7 for the Bayesian schemes and not for the Analogue reconstructions.

8

9 3. Results

10

11 In the following sub-sections we evaluate the ability of the different reconstruction techniques. In
12 subsection 3.1 we select a pseudo-proxy scenario with medium noise-level (equivalent to a
13 correlation with the target precipitation of 0.5) and evaluate the reconstruction schemes. In
14 subsection 3.2, we assess the impact of the noise in the pseudo-proxies time-series on the quality of
15 the reconstruction.

16

17 3.1. Evaluation of Reconstruction Techniques: Medium-noise pseudo-proxy 18 case

19

20 As measures of performance we present the three selected skill metrics (see 2.3 for details), and in
21 each case, we show the results at annual and at decadal resolution.

22

23 Figure 4 displays the Correlation Coefficient for the different reconstruction techniques. According
24 to this skill measure, regardless of the method and resolution, proxy-rich East China (EChina, 20N-
25 40N, 100E-120E) stands out as the best-reconstructed area. However, a fairly dense coverage by
26 proxy records seems not to be a universal indicator of success, as North-Western Arid China
27 (NWChina, 40N-50N, 72.5E-90E) is highlighted as an area where the Bayesian algorithms are
28 successful while the Analogue Method displays no ability. On the other hand, areas poorly covered
29 by the pseudo-proxy network (south of 18N, North-Eastern Asia and South of Tibet at longitudes
30 85E-95E) are the regions where the correlation coefficient is lowest.

31

32 For the annual-resolution reconstructions, the best performance is obtained by the BHM technique,
33 showing a spatial mean correlation with the target of 0.4 (Fig. 4a). Coupling the BHM with
34 clustering partially deteriorates the results, with the correlation coefficient severely dropping over

1 the proxy-rich EChina region (Fig. 4b and 4c). Meanwhile, the performance of the Analogue
2 Method is inferior: the Correlation Coefficient spatial mean is 0.25 and there is no skill in
3 reconstructing precipitation north of 42N despite the fact that pseudo-proxies are located in that
4 region (Fig. 4d).

5

6 For the decadal-resolved reconstructions the difference between the Bayesian methods and the
7 Analogue is even larger. In terms of the Correlation Coefficient measure the BHM (Analogue
8 Method) is the best (worst) performing with a spatial average of 0.37 (0.1). Among the Bayesian
9 schemes, the cluster coupling maintains the skill levels in all regions except India, where lower
10 correlation values are obtained. The Analogue Method shows a much constrained geographical
11 skill, with correlation values above 0.2 only over EChina and central India.

12

13 In general, for each of the methods, the Correlation Coefficient is higher for the annually-resolved
14 than for the decadal-resolved reconstruction. One exception to that is the BHM+5Clusters over
15 EChina. This behaviour is probably derived from the clustering division (see Figure A2).

16

17 Figure 5 shows the results for the RE index. In most of the grid-points the RE index is positive,
18 indicating a reduction of the error in comparison to forecasting the instrumental-period climatology
19 as reconstruction. For all the Bayesian methods and both time-resolutions the highest skill is found
20 in regions with high density of pseudo-proxy information. Again, the Analogue Method shows a
21 clear inferior performance over NWACHina, in spite of the considerable number of pseudo-proxy
22 locations present there.

23

24 For the annual reconstruction, improvements from climatology are found for the Bayesian
25 approaches in EChina, NWACHina, Mongolia and, to a lesser extent, in central India (Fig. 5a, 5b
26 and 5c). For the Analogue Method, the improvement with respect to climatology is confined only to
27 EChina and central India, and the improvement is weaker than with the Bayesian techniques (Fig.
28 5d).

29

30 For the decadal data, similar results are obtained. However, the RE index is notably negative in
31 some grid-points for the BHM+5clusters (mainly in the northern-most extent of the study region;
32 Fig. 5f) and the Analogue cases (everywhere with exception of EChina; Fig. 5h).

33

34 Figure 6 displays the results for the CRPS metric, for the probabilistic methods (Bayesian schemes).
35 For this metric, the annually-resolved (decadal-resolved) reconstructions have a CRPS of 190
36 mm/month (22 mm/month), compared to the target precipitation spatially-averaged standard
37 deviation of 34 mm/month (11 mm/month) for annual (decadal) data. This indicates that the

1 methods have more problems in reproducing the expected probability distribution functions in the
2 annual case.

3

4 For the annual resolution reconstructions there is almost no noticeable difference in the
5 performance of the three Bayesian schemes. For this metric, the region of best performance is
6 NWACHina. In this case, the performance over the proxy-rich EChina is intermediate (unlike with
7 the Correlation Coefficient and RE Index metrics). For the decadal resolution reconstructions, the
8 performance among the methods is quite different. While the spatial mean is in all the three cases
9 similar (around 22 mm/month), the spread among grid points is much higher for the
10 BHM+10Clusters scheme. In particular, for the 10 clusters scheme the skill over China and the
11 South-East of the study region is much higher than in the other methods. In general, the regions
12 with a dense proxy network display better performance levels and central India and the North-East
13 of the study area stand out as low-performing areas for all the three methodologies.

14

15 | Three main conclusions can be drawn from the experiments above: First, proxy-depleted areas can
16 not be successfully reconstructed. Second, the Bayesian schemes are superior to the Analogue
17 Method in all metrics (this difference is particularly acute over NWACHina where the Analogue
18 fails despite the relatively good coverage by proxy data). Third, among the Bayesian algorithms
19 there is no clear superiority results are similar, although a partial deterioration of the skill is detected
20 in some regions when clustering is coupled.-

21 |

22 | The under-performance of the Analogue method in comparison with the BHM variants might seem
23 in contradiction with the results of Gómez-Navarro et al. (2015), who do not find any significant
24 skill differences between these schemes. However, we should note an important difference between
25 the two studies: in Gómez-Navarro et al. (2015) the authors use as pool of analogues an
26 independent highly-resolved simulation performed with a regional model, while in this manuscript
27 we use the classical analogue approach based on the instrumental-period pool. This difference
28 makes it impossible to draw a fair comparison between the two studies, indicating that the pool of
29 analogues is essential for determining the potential success of the Analogue Method as
30 reconstruction technique.

31 |

32 | We hypothesise a couple of reasons for the failure of the Analogue Method over NWACHina: first,
33 the semi-arid precipitation regime dominant in the area and second an insufficient number of
34 analogues in the pool. As the method is unsuccessful both at annual and decadal resolutions we
35 think that the number of elements in the pool of analogues is not an important variable and that the
36 main cause for the failure resides in the fact that non-normal behaving time-series could potentially
37 be more difficult to mimic by analogues than Gaussian-behaving ones. However, providing a proof
38 for such hypothesis is out of the scope of this manuscript and will require the design of new
39 theoretical experiments with input data arising from different probability distributions.

1 |

2 | Disentangling the reasons leading to a partial deterioration of skill when coupling the BHM to
3 | Clustering algorithms will require additional experiments. However, we hypothesize that the main
4 | reason for such behaviour is related to the loss of information from geographical-neighbours. While
5 | during clustering geographical-neighbors can be separated, the information from such sites is taken
6 | into account in the covariance matrix structure of BHM and, therefore, losing information from
7 | close locations might affect the final performance.

8 3.2. Effect of noise in Pseudo-proxy records

9

10 Next, we evaluate the impact of noise in the pseudo-proxy time-series on the skill of the
11 reconstruction techniques. We focus on two schemes: one Bayesian (BHM+5Clusters, selected for
12 its balance between skill and computational requirements, as shown in subsection 3.1) and the
13 Analogue Method. We work with four noise levels for the pseudo-proxy time-series: high-noise
14 (correlation with truth: 0.3), medium-noise (correlation with truth: 0.5), low-noise (correlation with
15 truth: 0.7) and perfect-proxy (correlation with truth: 1). Note that the medium-noise proxies case
16 corresponds to the level used through sub-section 3.1. To simplify and summarize the results, in this
17 subsection we display the reconstructions performance in terms of only one skill measure: the
18 Correlation Coefficient.

19

20 Figure 7 shows the dependency of the Correlation Coefficient, averaged in space, with noise levels
21 in the pseudo-proxies records. At annual resolution, the skill of the methods increases in an almost
22 linear way with the quality of the pseudo-proxies records, except for a drop in the Bayesian skill in
23 the No-noise scenario. The BHM+5Clusters performance is better than the Analogue Method in all
24 cases except the No-noise one. For high-noise proxies the skill of the BHM+5Clusters (Analogue
25 Method) is 0.23 (0.18), while in the perfect-proxy scenario the BHM+5Clusters (Analogue Method)
26 reaches 0.30 (0.42). For decadal-resolved reconstructions the picture is quite different. The
27 Bayesian approaches show a quasi-constant skill for the medium, low and no noise examples
28 (around 0.33) and the Analogue Method performs poorly showing for all the noise types a skill
29 between 0.09 and 0.15. While for the Bayesian schemes the spatial average skill for the annual or
30 decadal resolutions is similar, the difference between annual versus decadal is important in the
31 Analogue case. To complement the spatially-averaged-information, Figures 8 and 9 show the
32 sensitivity of the correlation skill measure field to the noise-levels in the pseudo-proxies for the
33 BHM+5Clusters and the Analogue Method, respectively.

34

35 For the Bayesian algorithm (Fig. 8), the perfect-proxy case shows high performance over
36 NWACHina, EChina and North-East of the study area, at annual and decadal resolutions. For the
37 annual reconstruction, the skill of the scheme is low southward of 25N and over some grid cells in
38 the north of the area. For the decadal reconstruction, the same areas are also problematic and, in

1 addition, most of India is not well reconstructed. In general, as the noise level in the input pseudo-
2 proxies increases the performance of the method deteriorates and for the high-noise case only East
3 China and the NW of the study region show a moderate success.

4

5 Figure 9 presents the Analogue Method performance. For annual resolution, in the case of perfect
6 pseudo-proxies, the method is successful in the central part of the study area (between 15N and
7 45N), while the northern and southern most extremes are not well reconstructed. However, the
8 decadal counter-part is only skilful in EChina. In the high-noise end of the spectrum, the Analogue
9 Method only shows a satisfactory performance in EChina, between 20N-40N (25N-35N) for the
10 annually-resolved (decadally-resolved) reconstruction.

11

12 To summarize, as expected, the noise in the pseudo-proxy time-series is important ~~for the quality of~~
13 ~~the reconstruction~~, as the ~~latter quality of the reconstruction~~ rapidly decreases with the noise level.
14 ~~However, particularly for the decadal reconstructions, the reconstruction quality depends less on the~~
15 ~~noise level for the levels medium, high and no noise, as only minor differences are noticed.~~

16

17 4. Summary and Conclusions

18

19 This study evaluates the ability of several statistical techniques to reconstruct the precipitation field
20 over South-eastern Asia in a PPE setting. The reconstructions are performed using 1156 years of
21 model simulation (corresponding to the period 850-2005), at annual and at decadal resolution. The
22 techniques used are: BHM, BHM coupled with clustering (dividing South-eastern Asia into 5 or 10
23 clusters) and the Analogue Method. While the Analogue Method is a classical approach and has
24 been widely used, the Bayesian variants are novel for the hydro-climatological reconstructions'
25 field, being this the first time ~~results are reported for the Asian continent~~~~the technique is applied for~~
26 ~~Asian precipitation reconstruction.~~ Moreover, the coupling of the Bayesian modelling with
27 clustering algorithms is also an innovation that could potentially lead to a more wide-spread
28 application of these computationally-intensive processes.

29

30 We find that for all the algorithms and resolutions a high-density of pseudo-proxy information is a
31 necessary but not sufficient condition for a successful reconstruction. On one hand, the lack of
32 proxy data over regions such as the NE of the study area, south of Tibet and south of 20N,
33 determines that none of the methods is capable of delivering a skilful reconstruction. On the other
34 hand, a good performance over the proxy-rich areas of EChina and NWChina is not guaranteed
35 just by the amount of data present there: while all the methods are highly successful over EChina,
36 only the Bayesian algorithms deliver quality reconstructions over NWChina.

37

1 ~~We hypothesise a couple of reasons for the failure of the Analogue Method over NWACHina: first,~~
2 ~~the semi-arid precipitation regime dominant in the area and second an insufficient number of~~
3 ~~analogues in the pool. However, as the method is unsuccessful both at annual and decadal~~
4 ~~resolutions we think that the number of elements in the pool of analogues is not an important~~
5 ~~variable and that the main cause for the failure resides in the fact that non-normal behaving time-~~
6 ~~series are more difficult to mimic by analogues than Gaussian-behaving ones.~~

7
8 ~~-~~In general, for both the annual and the decadal reconstructions, while the Bayesian techniques are
9 superior to the Analogue Method, among the three Bayesian schemes the differences in skill are not
10 extremely notorious, although a partial deterioration of the skill is detected in some regions when
11 clustering is coupled. Noting that the Bayesian technique without any form of pre-clustering of the
12 area of interest (BHM) is extremely computationally expensive, coupling it with a clustering
13 scheme (BHM+5Clusters or BHM+10Clusters) seems to be a good compromise between success of
14 the reconstruction and computational demand (with computing times reduced up to 50%).

15
16 We also find that the quality of the final reconstructions is highly sensitive to the noise levels
17 included in the input pseudo-proxy data, being those variables negatively correlated. ~~However, for~~
18 ~~decadal resolutions the methods' performances are quite similar for levels of medium, low or no~~
19 ~~noise.~~ Only under a perfect-proxy (no-noise) scenario and at annual-resolution is the Analogue
20 Method capable of overperforming the Bayesian schemes over most areas. ~~However, e~~Even in this
21 ideal no-noise case NWACHina remains elusive for the Analogue methodology.

22
23 As a summary, we find that for millennium-length precipitation reconstructions over South-eastern
24 Asia a dense network of proxy information is mandatory for success, highlighting the complex
25 nature of the precipitation field in the area of study. Among the selected algorithms, the Bayesian
26 techniques perform generally better than the Analogue Method, being the difference in abilities
27 highest over the semi-arid Northwest and in the decadal-resolution framework. The superiority of
28 the Bayesian approach indicates that directly modelling the space and time precipitation field
29 variability encapsulates more added value is more appropriate than just relying in similarities within
30 a restricted pool of observational analogues, in which certain regimes might not be present.

31
32 A natural next step is to implement real-world reconstructions of precipitation in the region of
33 continental South-eastern Asia. These PPE are auspicious for such a future endeavour, as some
34 moderate skill can be expected in most of the region. Nevertheless, it is important to acknowledge
35 that these experiments are highly idealised and that real-world data might incorporate additional
36 constraints and challenges. ~~-~~Additionally, more PPE could be also designed lifting some of the
37 simplifications assumed here. For example, while here we only took proxy time-series that cover
38 the whole period of interest, with the same temporal resolution, same signal to noise relation and
39 same relationship with the underlying hydroclimatic variable of interest, some of these constrains

1 could be modified to better resemble reality.

2

3 **Acknowledgements**

4 ST, LS and JL are supported by the Belmont Forum and JPI-Climate Collaborative Research Action
5 “INTEGRATE: An integrated data-model study of interactions between tropical monsoons and
6 extratropical climate variability and extremes”. [JL acknowledges support by the UK–China
7 Research and Innovation Partnership Fund through the Met Office Climate Science for Service
8 Partnership China \(CSSP\) as part of the Newton Fund.](#)

9 [The authors thank the reviewers for constructive criticism and suggestions that improved the quality
10 of the paper.](#)
11

12 **5. References**

13

14 Cai, Y., Tan, L., Cheng, H., An, Z., Edwards, R.L., Kelly, M.J., Kong, X. and Wang, X.: The
15 variation of summer monsoon precipitation in central China since the last deglaciation, *Earth
16 Planet. Sci. Lett.* 291, 21–31, doi: 10.1016/j.epsl.2009.12.039, 2010.

17

18 Chen, J., Chen, F., Feng, S., Huang, W., Liu, J., and Zhou, A.: Hydroclimatic changes in China and
19 surroundings during the Medieval Climate Anomaly and Little Ice Age: spatial patterns and possible
20 mechanisms, *Quat. Sci. Rev.*, 107, 98-111, doi: 10.1016/j.quascirev.2014.10.012, 2015

21

22 Chu, G., Sun, Q., Wang, X., Li, D., Rioual, P., Qiang, L., Han, J. and Liu, J.: A 1600 year
23 multiproxy record of paleoclimatic change from varved sediments in Lake Xiaolongwan,
24 northeastern China, *J. Geophys. Res.* 114, doi: 10.1029/2009JD012077, 2009

25

26 Cook, E. R., Briffa, K. R., and Jones, P. D.: Spatial regression methods in dendroclimatology: a
27 review and comparison of two techniques, *Int. J. Climatol.*, 14(4), 379-402, doi:
28 10.1002/joc.3370140404, 1994.

29

30 Cook, E. R., Anchukaitis, K. J., Buckley, B. M., D’Arrigo, R. D., Jacoby, G. C., & Wright, W. E. X:
31 Asian monsoon failure and megadrought during the last millennium. *Science*, 328(5977), 486-489,
32 | 2010.

33 |

34 Feng, S., Hu, Q., Wu, Q., and Mann, M. E.: A gridded reconstruction of warm season precipitation
35 for Asia spanning the past half millennium, *J. Clim.*, 26(7), 2192-2204, doi: 10.1175/JCLI-D-12-

1 00099.1,2013.

2

3 Feng, Z.-D., Wu, H.N., Zhang, C.J., Ran, M. and Sun, A.Z.: Bioclimatic change of the past 2500
4 years within the Balkhash Basin, eastern Kazakhstan, Central Asia, *Quat. Int.* 311, 63–70. doi:
5 10.1016/j.quaint.2013.06.032, 2013.

6

7 Franke, J., González-Rouco, J. F., Frank, D., and Graham, N. E.: 200 years of European temperature
8 variability: insights from and tests of the proxy surrogate reconstruction analog method, *Clim. Dyn.*,
9 37(1-2), 133-150, doi: 10.1007/s00382-010-0802-6, 2011.

10

11 Gelman A, Carlin J, Stern H and Rubin D: *Bayesian Data Anal*, 3rd edn, Chapman and Hall,
12 London, 2003.

13

14 Gómez-Navarro, J. J., Werner, J., Wagner, S., Luterbacher, J., and Zorita, E.: Establishing the skill
15 of climate field reconstruction techniques for precipitation with pseudoproxy experiments, *Clim.*
16 *Dyn.*, 45(5-6), 1395-1413, doi: 10.1007/s00382-014-2388-x, 2015.

17

18 Gong, G. and Hameed, S.: The variation of moisture conditions in China during the last 2000 years,
19 *Int. J. Climatol.* 11, 271–283, doi: 10.1002/joc.3370110304, 1991.

20

21 Gou, X., Deng, Y., Chen, F., Yang, M., Fang, K., Gao, L., Yang, T., Zhang, F.: Tree ring based
22 streamflow reconstruction for the Upper Yellow River over the past 1234 years, *Chin. Sci. Bull.* 55,
23 4179–418, doi: 10.1007/s11434-010-4215-z, 2010.

24

25 Guillot D, Rajaratnam B and Emile-Geay J: Statistical paleoclimate reconstructions via Markov
26 random fields, *Ann. Appl. Stat.* 9 324–52, doi:10.1214/14-AOAS794, 2015.

27

28 He, M., Bräuning, A., Griesinger, J., Hochreuther, P., and Wernicke, J.: May–June drought
29 reconstruction over the past 821 years on the south-central Tibetan Plateau derived from tree-ring
30 width series, *Dendrochronologia*, 47, 48-57, doi: 10.1016/j.dendro.2017.12.006, 2018.

31

32 He, Y., Zhao, C., Wang, Z., Wang, H., Song, M., Liu, W. and Liu, Z.: Late Holocene coupled
33 moisture and temperature changes on the northern Tibetan Plateau, *Quat. Sci. Rev.* 80, 47–57. doi:
34 10.1016/j.quascirev.2013.08.017, 2013.

1

2 Hershbach, H.: Decomposition of the continuous ranked probability score for ensemble prediction
3 systems, *Weather Forecasting*, 15(5), 559-570, doi: 10.1175/1520-
4 0434(2000)015<0559:DOTCRP>2.0.CO;2, 2000.

5

6 Hong, Y.T., Hong, B., Lin, Q.H., Shibata, Y., Hirota, M., Zhu, Y.X., Leng, X.T., Wang, Y., Wang, H.
7 and Yi, L.: Inverse phase oscillations between the East Asian and Indian Ocean summer monsoons
8 during the last 12000 years and paleo-El Niño, *Earth Planet. Sci. Lett.* 231, 337–346. doi:
9 10.1016/j.epsl.2004.12.025, 2005.

10

11 Hu, C., Henderson, G.M., Huang, J., Xie, S., Sun, Y. and Johnson, K.R.: Quantification of Holocene
12 Asian monsoon rainfall from spatially separated cave records, *Earth Planet. Sci. Lett.* 266, 221–232.
13 doi: 10.1016/j.epsl.2007.10.015, 2008.

14

15 Izenman A.J.: *Modern Multivariate Statistical Techniques*, Springer Texts in Statistics, 2008.

16

17 Jiang, T., Zhang, Q., Blender, R. and Fraedrich, K.: Yangtze Delta floods and droughts of the last
18 millennium: Abrupt changes and long term memory, *Theor. Appl. Climatol.* 82, 131–141, doi:
19 10.1007/s00704-005-0125-4, 2005

20

21 Jones, P.D., Briffa, K.R., Osborn, T.J., Lough, J.M., van Ommen, T.D., Vinther, B.M., Luterbacher,
22 J., Wahl, E., Zwiers, F.W., Schmidt, G.A., Ammann, C., Mann, M.E., Buckley, B.M., Cobb, K.,
23 Esper, J., Goosse, H., Graham, N., Jansen, E., Kiefer, T., Kull, C., Küttel, M., Mosley-Thompson,
24 E., Overpeck, J.T., Riedwyl, N., Schulz, M., Tudhope, S., Villalba, R., Wanner, H., Wolff, E., and
25 Xoplaki, E.: High-resolution palaeoclimatology of the last millennium: a review of current status
26 and future prospects, *Holocene*, 19, 3-49, doi: 10.1177/0959683608098952, 2009.

27

28 Jones, M.D., Roberts, C.N., Leng, M.J. and Türkeş, M.: A high-resolution late Holocene lake
29 isotope record from Turkey and links to North Atlantic and monsoon climate, *Geol.* 34, 361. doi:
30 10.1130/G22407.1, 2006.

31

32 Kasper, T., Haberzettl, T., Doberschütz, S., Daut, G., Wang, J., Zhu, L., Nowaczyk, N. and
33 Mäusbacher, R.: Indian Ocean Summer Monsoon (IOSM)-dynamics within the past 4 ka recorded
34 in the sediments of Lake Nam Co, central Tibetan Plateau (China), *Quat. Sci. Rev.* 39, 73–85, doi:
35 10.1016/j.quascirev.2012.02.011, 2012.

1

2 Kuo, T.S., Liu, Z.Q., Li, H.C., Wan, N.J., Shen, C.C. and Ku, T.L.: Climate and environmental
3 changes during the past millennium in central western Guizhou, China as recorded by Stalagmite
4 ZJD-21, *J. Asian Earth Sci.* 40, 1111–1120, doi: 10.1016/j.jseaes.2011.01.001, 2011.

5

6 Lamy, F., Arz, H.W., Bond, G.C., Bahr, A. and Pätzold, J.: Multicentennial-scale hydrological
7 changes in the Black Sea and northern Red Sea during the Holocene and the Arctic/North Atlantic
8 Oscillation: HOLOCENE BLACK AND RED SEA, *Paleoceanogr.* 21, doi:
9 10.1029/2005PA001184, 2006.

10

11 Li, H.C., Lee, Z.H., Wan, N.J., Shen, C.C., Li, T.Y., Yuan, D.X. and Chen, Y.H.: The $\delta^{18}\text{O}$ and
12 $\delta^{13}\text{C}$ records in an aragonite stalagmite from Furong Cave, Chongqing, China: A-2000-year record
13 of monsoonal climate, *J. Asian Earth Sci.* 40, 1121–1130, doi: 10.1016/j.jseaes.2010.06.011, 2011.

14

15 Liu, J., Chen, F., Chen, J., Xia, D., Xu, Q., Wang, Z. and Li, Y.: Humid medieval warm period
16 recorded by magnetic characteristics of sediments from Gonghai Lake, Shanxi, North China, *Chin.*
17 *Sci. Bull.* 56, 2464–2474, doi: 10.1007/s11434-011-4592-y, 2011.

18

19 Liu, Z., Liu, Q., Torrent, J., Barrón, V., and Hu, P.: Testing the magnetic proxy $\chi_{\text{FD}}/\text{HIRM}$ for
20 quantifying paleoprecipitation in modern soil profiles from Shaanxi Province, China, *Global*
21 *Planet. Change*, 110, 368-378, doi: 10.1016/j.gloplacha.2013.04.013, 2013.

22

23 Liu, X., Dong, H., Yang, X., Herzschuh, U., Zhang, E., Stuut, J.-B.W. and Wang, Y.: Late Holocene
24 forcing of the Asian winter and summer monsoon as evidenced by proxy records from the northern
25 Qinghai–Tibetan Plateau, *Earth Planet. Sci. Lett.* 280, 276–284, doi: 10.1016/j.epsl.2009.01.041,
26 2009.

27

28 Liu, X., Herzschuh, U., Shen, J., Jiang, Q. and Xiao, X.: Holocene environmental and climatic
29 changes inferred from Wulungu Lake in northern Xinjiang, China, *Quat. Res.* 70, 412–425, doi:
30 10.1016/j.yqres.2008.06.005, 2008.

31

32 Ljungqvist, F. C., Krusic, P. J., Sundqvist, H. S., Zorita, E., Brattström, G., and Frank, D.: Northern
33 Hemisphere hydroclimate variability over the past twelve centuries, *Nat.*, 532(7597), 94,
34 doi:10.1038/Nat.17418, 2016

35

- 1 Luterbacher, J., Werner, J. P., Smerdon, J. E., Fernández-Donado, L., González-Rouco, F. J.,
2 Barriopedro, D., ... and Esper, J.: European summer temperatures since Roman times, *Environ. Res.*
3 *Lett.*,11(2), 024001, doi:10.1088/1748-9326/11/2/024001, 2016.
- 4
- 5 Luterbacher, J., and Zorita, E.: Spatial climate field reconstructions. In: White, S., Pfister, C. and
6 Mauelshagen, F. (Eds), *The Palgrave Handbook of Climate History*. Palgrave Macmillan UK, 131-
7 139, 2018.
- 8
- 9 Mann, M. E., and Rutherford, S.: Climate reconstruction using ‘Pseudoproxies’, *Geophys. Res.*
10 *Lett.*, 29(10), 139-1, doi: 10.1029/2001GL014554, 2002.
- 11
- 12 Nilsen, J.P. Werner, D.V. Divine, M. Rypdal: Assessing the performance of the BARCAST climate
13 field reconstruction technique for a climate with long-range memory, *Clim. Past* 14 (6), 947-967,
14 doi: 10.5194/cp-14-947-2018, 2018.
- 15
- 16 Oberhänsli, H., Novotná, K., Píšková, A., Chabrillat, S., Nourgaliev, D.K., Kurbaniyazov, A.K. and
17 Matys Grygar, T.: Variability in precipitation, temperature and river runoff in W Central Asia during
18 the past ~2000yrs, *Glob. Planet. Change* 76, 95–104. doi: 10.1016/j.gloplacha.2010.12.008, 2011.
- 19
- 20 Otto-Bliesner, B.L., Brady, E.C., Fasullo, J., Jahn, A., Landrum, L., Stevenson, S., ... and Strand,
21 G.: Climate variability and change since 850 CE: An ensemble approach with the Community
22 Earth System Model, *Bull. Am. Meteorol. Soc.*, 97(5), 735-754, doi: 10.1175/BAMS-D-14-00233.1,
23 2016.
- 24
- 25 Paulsen, D.E., Li, H.C. and Ku, T.L.: Climate variability in central China over the last 1270 years
26 revealed by high-resolution stalagmite records, *Quat. Sci. Rev.* 22, 691–701, doi: 10.1016/S0277-
27 3791(02)00240-8, 2003.
- 28
- 29 Qian, W., Hu, Q., Zhu, Y., Lee, D.K.: Centennial-scale dry-wet variations in East Asia, *Clim. Dyn.*
30 21, 77–89, doi: 10.1007/s00382-003-0319-3, 2003.
- 31
- 32 Sanwal, J., Kotlia, B.S., Rajendran, C., Ahmad, S.M., Rajendran, K. and Sandiford, M.: Climatic
33 variability in Central Indian Himalaya during the last ~1800 years: Evidence from a high resolution
34 speleothem record, *Quat. Int.* 304, 183–192, doi: 10.1016/j.quaint.2013.03.029, 2013.
- 35

1 Schneider, T.: Analysis of incomplete climate data: Estimation of mean values and covariance
2 matrices and imputation of missing values, *J. Clim.*, 14(5), 853-871, doi: 10.1175/1520-
3 0442(2001)014<0853:AOICDE>2.0.CO;2, 2001.

4

5 Sheppard, P.R., Tarasov, P.E., Graumlich, L.J., Heussner, K.U., Wagner, M., Sterle, H., Thompson,
6 L.G.: Annual precipitation since 515 BC reconstructed from living and fossil juniper growth of
7 northeastern Qinghai Province, China, *Clim. Dyn.* 23, 869–881, doi: 10.1007/s00382-004-0473-2,
8 2004.

9

10 Shi, F., Li, J., and Wilson, R.J.: A tree-ring reconstruction of the South Asian summer monsoon
11 index over the past millennium, *Sci. Rep.*, 4, 6739, doi: 10.1038/srep06739, 2014.

12

13 Shi, F., Guo, Z., Goosse, H., and Yin, Q.: Multi-proxy reconstructions of precipitation field in China
14 over the past 500 years, *Clim. Past*, 13, doi: 10.5194/cp-13-1919-2017, 2017.

15

16 Sinha, A., Berkelhammer, M., Stott, L., Mudelsee, M., Cheng, H. and Biswas, J.: The leading mode
17 of Indian Summer Monsoon precipitation variability during the last millennium: INDIAN
18 SUMMER MONSOON VARIABILITY, *Geophys. Res. Lett.* 38, doi: 10.1029/2011GL047713,
19 2011.

20

21 Smerdon, J.E.: Climate models as a test bed for climate reconstruction methods: pseudoproxy
22 experiments, *Wiley Interdisciplinary Reviews: Clim. Change*, 3(1), 63-77, doi: 10.1002/wcc.149,
23 2012.

24

25 Smerdon, J. E., Kaplan, A., Chang, D., & Evans, M. N.: A pseudoproxy evaluation of the CCA and
26 RegEM methods for reconstructing climate fields of the last millennium. *J Clim.* ,23(18), 4856-
27 4880, 2010.

28

29 Sorrel, P., Popescu, S.-M., Head, M.J., Suc, J.P., Klotz, S. and Oberhänsli, H.: Hydrographic
30 development of the Aral Sea during the last 2000 years based on a quantitative analysis of
31 dinoflagellate cysts, *Palaeogeogr. Palaeoclimatol. Palaeoecol.* 234, 304–327, doi:
32 10.1016/j.palaeo.2005.10.012, 2006.

33

34 Sun, A. and Feng, Z.: Holocene climatic reconstructions from the fossil pollen record at Qigai Nuur
35 in the southern Mongolian Plateau, *The Holocene* 23, 1391–1402, doi:

1 10.1177/0959683613489581, 2013.

2

3 Tan, L., Yanjun Cai, Zhisheng An, Edwards, R.L., Hai Cheng, Shen, C.C., Haiwei Zhang:
4 Centennial- to decadal-scale monsoon precipitation variability in the semi-humid region, northern
5 China during the last 1860 years: Records from stalagmites in Huangye Cave, *The Holocene*, 21,
6 287–296, doi: 10.1177/0959683610378880, 2011.

7

8 Tan, L., Yanjun Cai, Liang Yi, Zhisheng An, Li Ai: Precipitation variations of Longxi, northeast
9 margin of Tibetan Plateau since AD 960 and their relationship with solar activity, *Clim. Past* 4, 19–
10 28, doi: 10.5194/cp-4-19-2008, 2008.

11

12 Tingley, M. P., and Huybers, P.: A Bayesian algorithm for reconstructing climate anomalies in space
13 and time. Part I: Development and applications to paleoclimate reconstruction problems, *J. Clim.*,
14 23(10), 2759-2781, doi: 10.1175/2009JCLI3015.1, 2010.

15

16 Tingley, M. P., and Huybers, P.: Recent temperature extremes at high northern latitudes
17 unprecedented in the past 600 years, *Nat.*, 496(7444), 201, doi: 10.1038/Nat.11969, 2013.

18

19 Treydte, K.S., Schleser, G.H., Helle, G., Frank, D.C., Winiger, M., Haug, G.H. and Esper, J.: The
20 twentieth century was the wettest period in northern Pakistan over the past millennium, *Nat.*, 440,
21 1179–1182, doi: 10.1038/Nat.04743, 2006.

22

23 von Rad, U., Schaaf, M., Michels, K.H., Schulz, H., Berger, W.H. and Sirocko, F.: A 5000-yr
24 Record of Clim. Change in Varved Sediments from the Oxygen Minimum Zone off Pakistan,
25 Northeastern Arabian Sea, *Quat. Res.* 51, 39–53, doi: 10.1006/qres.1998.2016, 1999.

26

27 Wang, Z., Li, Y., Liu, B., and Liu, J.: Global climate internal variability in a 2000-year control
28 simulation with Community Earth System Model (CESM), *Chinese Geog. Sci.*, 25(3), 263-273, doi:
29 10.1007/s11769-015-0754-1, 2015.

30

31 Wang, Y., Cheng, H., Edwards, R.L., He, Y., Kong, X., An, Z.S., Wu, J., Kelly, M.J., Dykoski, C.A.,
32 Li, X.: The Holocene Asian Monsoon: Links to Solar Changes and North Atlantic Climate, *Sci.*,
33 308, 854–857, doi: 10.1126/science.1106296, 2005.

34

- 1 Wang, Wei, Feng, Z., Ran, M., Zhang, C.: Holocene climate and vegetation changes inferred from
2 pollen records of Lake Aibi, northern Xinjiang, China: A potential contribution to understanding of
3 Holocene climate pattern in East-central Asia, *Quat. Int.* 311, 54–62, doi:
4 10.1016/j.quaint.2013.07.034, 2013.
- 5
- 6 Werner, J.P., Luterbacher, J., and Smerdon, J.E.: A Pseudoproxy Evaluation of Bayesian
7 Hierarchical Modelling and Canonical Correlation Analysis for Climate Field Reconstructions over
8 Europe, *J. Clim.*, 26, 851–867, doi: 10.1175/JCLI-D-12-00016.1, 2013.
- 9
- 10 Werner, J. P., Divine, D. V., Ljungqvist, F. C., Nilsen, T., and Francus, P.: Spatio-temporal
11 variability of Arctic summer temperatures over the past 2 millennia, *Clim. Past*, 14(4), 527, 2018.
- 12
- 13 Wilks: *Statistical Methods in the Atmospheric Sciences*, 2011.
- 14
- 15 Yan, Z., Li, Z. and Wang, X.: An analysis of decade-to century-scale climatic jumps in history,
16 *Sci. Atmos. Sin.* 17, 663–672, 1993.
- 17
- 18 Yang, B., Qin, C., Shi, F., Sonechkin, D.M.: Tree ring-based annual streamflow
19 reconstruction for the Heihe River in arid northwestern China from AD 575 and its implications for
20 water resource management, *The Holocene* 22, 773–784, doi: 10.1177/0959683611430411, 2012.
- 21
- 22 Yang, B., Qin, C., Wang, J., He, M., Melvin, T.M., Osborn, T.J. and Briffa, K.R.: A 3,500-year tree-
23 ring record of annual precipitation on the northeastern Tibetan Plateau, *Proc. Natl. Acad. Sci.* 111,
24 2903–2908, doi: 10.1073/pnas.1319238111, 2014.
- 25
- 26 Yao, T. et al.: Variations in temperature and precipitation in the past 2000 a on the Xizang
27 (Tibet) Plateau – Guliya ice core record, *Sci. China Ser. D-Earth Sci.* 39, 425–433, 1996.
- 28
- 29 Yu, X., Zhou, W., Franzen, L.G., Xian, F., Cheng, P., Jull, A.J.T.: High-resolution peat records for
30 Holocene monsoon history in the eastern Tibetan Plateau, *Sci. China Ser. D* 49, 615–621, doi:
31 10.1007/s11430-006-0615-y, 2006.
- 32
- 33 Zeng, Y., Chen, J., Zhu, Z., Li, J., Wang, J. and Wan, G.: The wet Little Ice Age recorded by

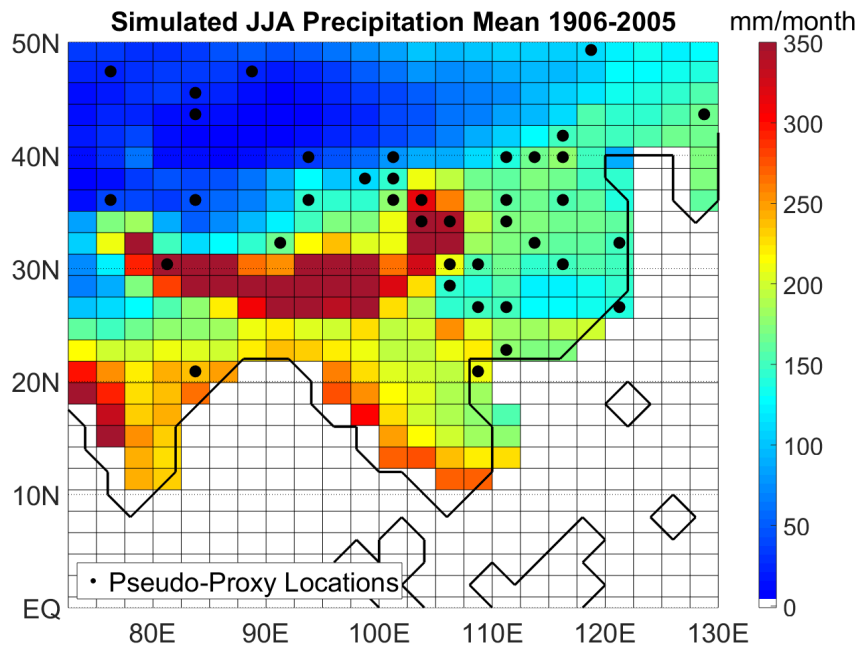
- 1 sediments in Huguangyan Lake, tropical South China, *Quat. Int.* 263, 55–62, doi:
2 10.1016/j.quaint.2011.12.022, 2012.
- 3
- 4 Zhai, D., Xiao, J., Zhou, L., Wen, R., Chang, Z., Wang, X., Jin, X., Pang, Q. and Itoh, S.: Holocene
5 East Asian monsoon variation inferred from species assemblage and shell chemistry of the
6 ostracodes from Hulun Lake, Inner Mongolia, *Quat. Res.* 75, 512–522, doi:
7 10.1016/j.yqres.2011.02.008, 2011.
- 8
- 9 Zhang, H., Werner, J.P., García-Bustamante, E., González-Rouco, F.J., Wagner, S., Zorita, E.,
10 Fraedrich, K., Jungclaus, J., Zhu, X., Xoplaki, E., Chen, F., Duan, J., Ge, Q., Hao, Z., Ivanov, M.,
11 Talento, S., Schneider, L., Wang, J., Yang, B., and Luterbacher, J.: East Asian warm season
12 temperature variations over the past two millennia, *Nat. Sci. Reports*, 8, 7702, doi:10.1038/s41598-
13 018-26038-8, 2018.
- 14
- 15 Zhang, Y., Tian, Q., Gou, X., Chen, F., Leavitt, S.W. and Wang, Y. Annual precipitation
16 reconstruction since AD 775 based on tree rings from the Qilian Mountains, northwestern China,
17 *Int. J. Climatol.* 31, 371–381, doi: 10.1002/joc.2085, 2011.
- 18
- 19 Zhang, Q., Gemmer, M. and Chen, J.: Clim. Changes and flood/drought risk in the Yangtze Delta,
20 China, during the past millennium, *Quat. Int.* 176–177, 62–69, doi: 10.1016/j.quaint.2006.11.004,,
21 2008.
- 22
- 23 Zheng, J., Wang, W.-C., Ge, Q., Man, Z. and Zhang, P.: Precipitation Variability and Extreme
24 Events in Eastern China during the Past 1500 Years, *Terr. Atmospheric Ocean. Sci.* 17, 579, doi:
25 10.3319/TAO.2006.17.3.579(A), 2006.

1 Table 1: List of the real-world Proxy records used to select the locations of the pseudo-proxy
 2 network.

3

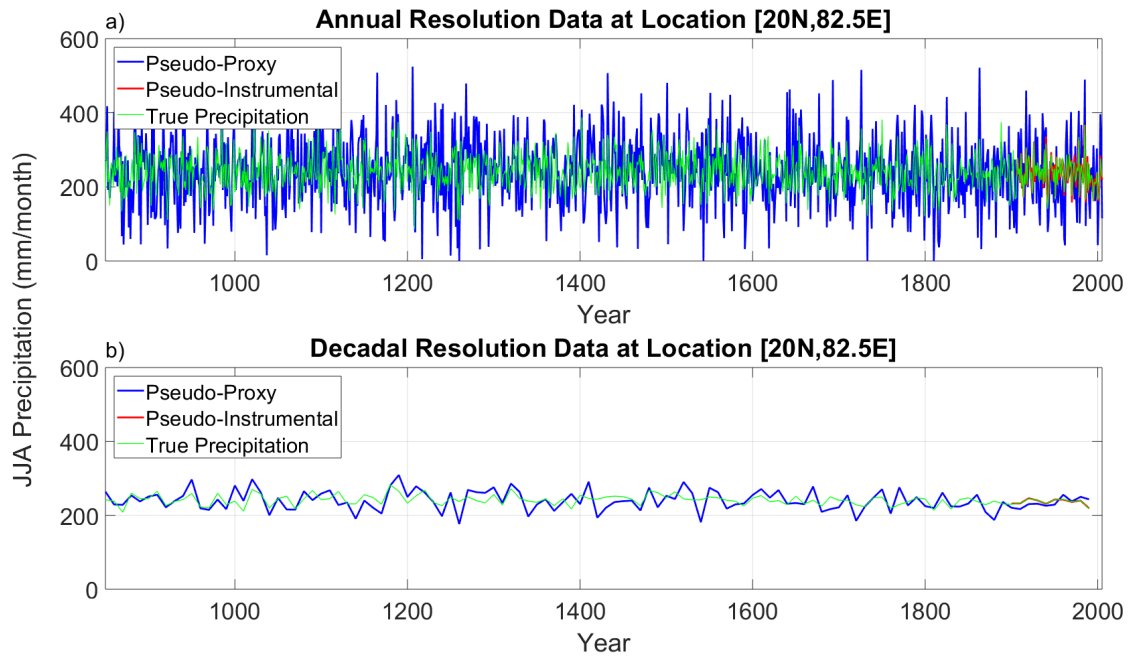
	Site	Longitude	Latitude	Archive	Target Season	Reference
1	Anyemaqen Mountains	99.5	34.5	Tree	Annual	Gou et al, 2010
2	Balkhash Basin	75	46.9	Pollen	Annual	Feng et al., 2013
3	Buddha Cave	109.5	33.4	Speleothem	Annual	Paulsen et al., 2003
4	Central India Composite	82	19	Speleothem	Summer	Sinha et al., 2011
5	Delingha	97.38	37.38	Tree	Annual	Yang et al., 2014
6	Dharamjali Cave	80.21	29.52	Speleothem	Annual	Sanwal et al., 2013
7	Dongge Cave	108.8	25.28	Speleothem	Annual	Wang et al., 2005
8	Eastern Tibetan Plateau	102.52	32.77	Lake	Annual	Yu et al., 2006
9	Furong Cave	107.9	29.29	Speleothem	Summer	Li et al, 2011
10	Gonghai Lakee	112.23	38.9	Lake	Summer	Liu et al, 2011
11	Great Bend of the Yellow River	115	35	Documentary	Annual	Gong and Hamed 1991
12	Guliya	81.48	35.28	Ice	Annual	Yao et al., 1996
13	Haihe River Basin	116	40	Documentary	Annual	Yan et al., 1993
14	Hani	126.51	42.21	Lake	Annual	Hong et al., 2005
15	Heihe River Basin	100	38.2	Tree	Annual	Yang et al., 2012
16	Heshang_Cave	109.36	19.41	Speleothem	Annual	Hu et al., 2008
17	Huangye Cave	105.12	33.92	Speleothem	Annual	Tan et al., 2011
18	Huguangyan Lakee	110.28	21.15	Lake	Annual	Zeng et al., 2012
19	Jianghuai	113.5	31.5	Documentary	Annual	Zheng et al., 2006
20	Jiangnan	115	30	Documentary	Annual	Zheng et al., 2006
21	Jiuxian Cave	109.1	33.57	Speleothem	Summer	Cai et al., 2010
22	Karakorum Mountains	74.93	35.9	Tree	Annual	Treedyte et al., 2006
23	Kesang Cave	81.75	42.87	Speleothem	Annual	Zheng et al., 2012

24	Kusai Lake	93.25	35.4	Lake	Summer	Liu et al., 2009
25	Lake Aibi	82.84	44.9	Lake	Annual	Wang et al., 2013
26	Lake Gahai	102.33	34.24	Lake	Annual	He et al., 2013
27	Lake Hulun	117.5	49	Lake	Annual	Zhai et al., 2011
28	Lake Nam Co	90.78	30.73	Lake	Summer	Kasper et al., 2012
29	Lake Xiaolongwan	126.35	42.3	Lake	Annual	Chu et al., 2009
30	Lonxi Area	105	30	Documentary	Annual	Tan et al., 2008
31	North China Plains	115	38	Documentary	Annual	Zheng et al., 2006
32	North-eastern Tibetan Plateau	98	37	Tree	Annual	Yang et al., 2014
33	Qaidam Basin	97.5	37.2	Tree	Annual	Yin et al., 2008
34	Qaidam Basin	97.5	37.2	Tree	Annual	Wang et al., 2013
35	Qigai Nuur	109.5	39.5	Pollen	Annual	Sun et al., 2013
36	Qilian Mountains	99.5	38.5	Tree	Annual	Zhang et al., 2011
37	Qinghai Province	99	37	Tree	Annual	Sheppard et al., 2004
38	Southern China	110	25	Documentary	Annual	Qian et al., 2003
39	Sugan Lake	93.9	38.85	Lake	Annual	He et al., 2013
40	Tsuifong Lake	121.6	24.5	Lake	Annual	Wang et al., 2013
41	Wanxiang Cave	105	33.19	Speleothem	Annual	Zhang et al., 2008
42	Wulungu Lake	87.15	47.15	Pollen	Annual	Liu et al., 2008
43	Yangtze Delta	121	32	Documentary	Annual	Zhang et al., 2008
44	Yangtze Delta	120	32	Documentary	Annual	Jiang et al., 2005
45	Yangtze Delta	115	30	Documentary	Annual	Qian et al., 2003
46	Yellow River	110	35	Documentary	Annual	Qian et al., 2003
47	Zhijin Cave	105.84	26.73	Speleothem	Summer	Kuo et al., 2011



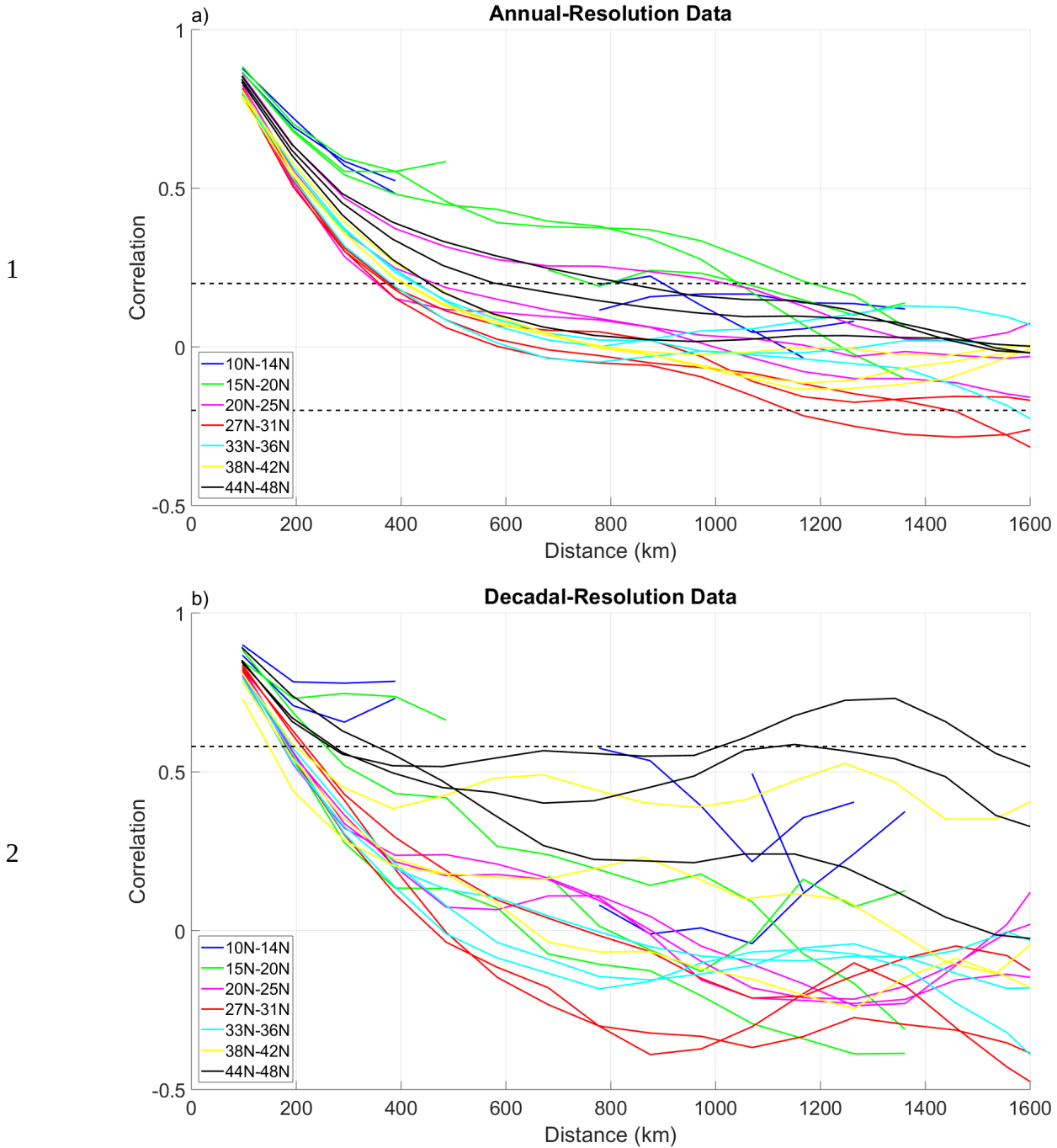
1

2 **Figure 1: Simulated mean JJA precipitation (mm/month) during the instrumental period**
 3 **(years 1906-2005) in over continental Asia. BlackMagenta dots: Pseudo-Proxy network.**



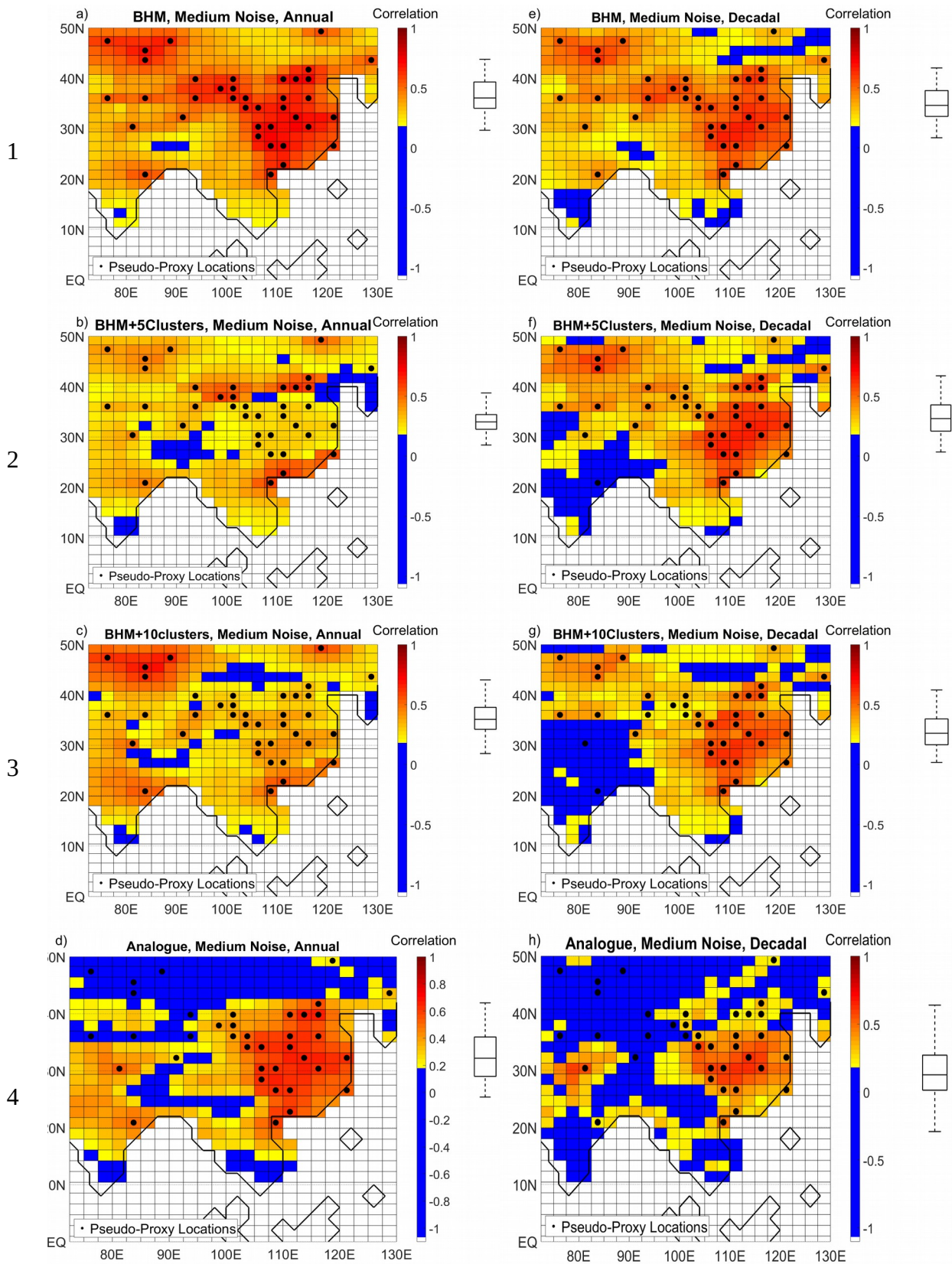
1

2 **Figure 2: Example of Pseudo-Proxy, Pseudo-Instrumental and True precipitation time-series**
3 **at location [20N,82.5E]. a) Annually-resolved data b) Decadally-resolved data.**

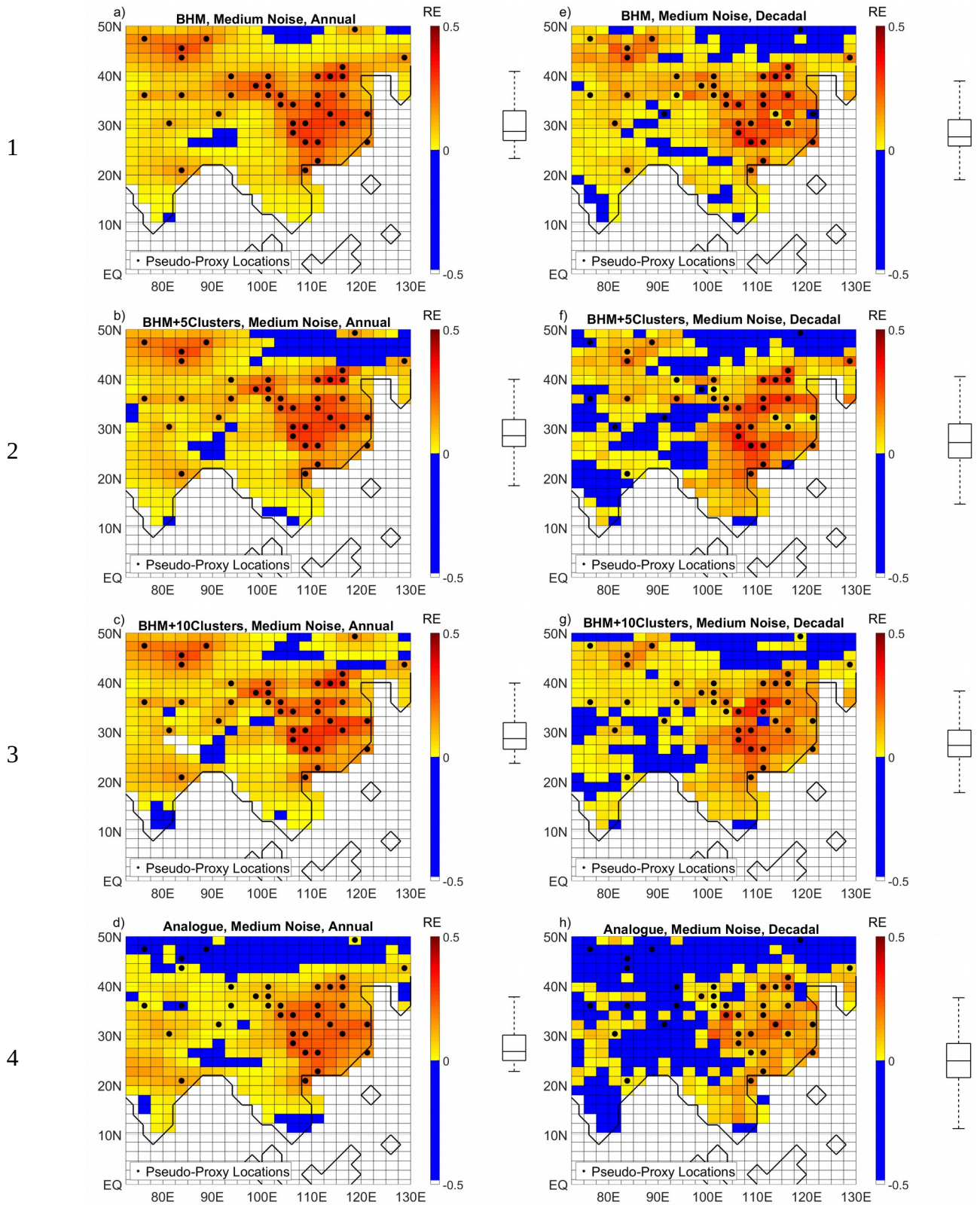


3 **Figure 3: Correlation of Simulated JJA precipitation time-series across different latitudinal**
 4 **bands, versus distance. Only the instrumental period (years 1906-2005) and the grid-points in**
 5 **continental Asia are considered for the calculation. a) Annual-resolution Data, b) Decadal-**
 6 **resolution Data. Dashed horizontal lines indicate the thresholds of statistical significance at a**
 7 **95% confidence level according to the t-student test.**

8 **For this plot, all grid-points in the same latitude band are grouped together and then one-to-**
 9 **one correlations are calculated between members of the same group.**



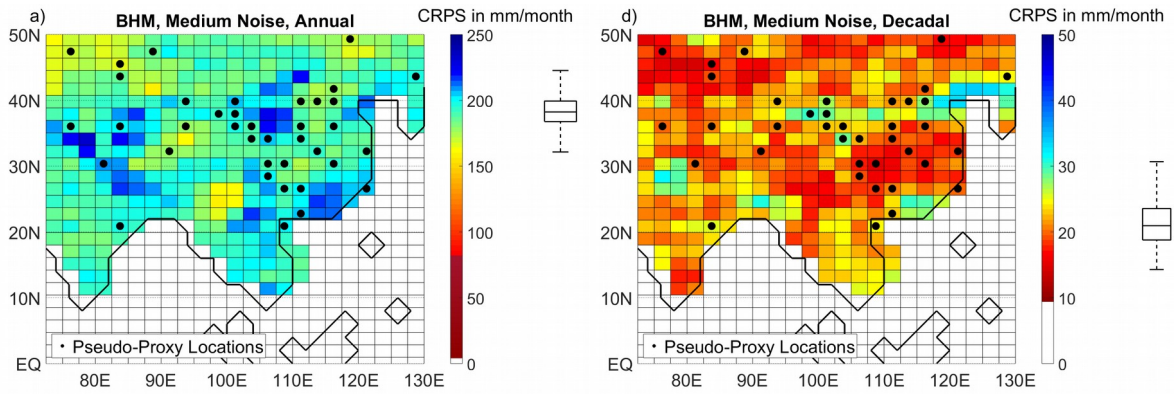
5 **Figure 4: Correlation between Target Precipitation and different Reconstructions, at each**
 6 **grid point. Left: Annually-resolved data. Right: Decadally-resolved data.**
 7 **a and e: BHM. b and f: BHM + 5Clusters. c and g: BHM + 10 Clusters. d and h: Analogue**
 8 **Method. The boxplots (indicating median, 25% and 75% percentiles and non-outlier limits)**
 9 **to the right of the colour bars show the distribution of the grid point Correlation Coefficients.**



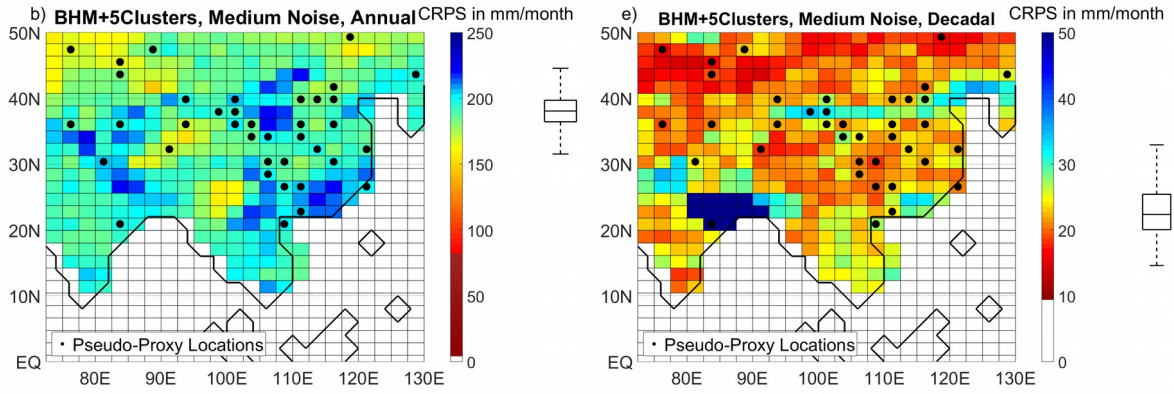
5 **Figure 5: RE Index for different Reconstructions, at each grid point. Left: Annually-resolved**
 6 **data. Right: Decadally-resolved data. a and e: BHM. b and f: BHM + 5Clusters. c and g:**
 7 **BHM + 10 Clusters. d and h: Analogue Method. The boxplots (indicating median, 25% and**
 8 **75% percentiles and non-outlier limits) to the right of the colour bars show the distribution**
 9 **of the grid point RE Index.**

10 **Black dots: Pseudo-Proxy network.**

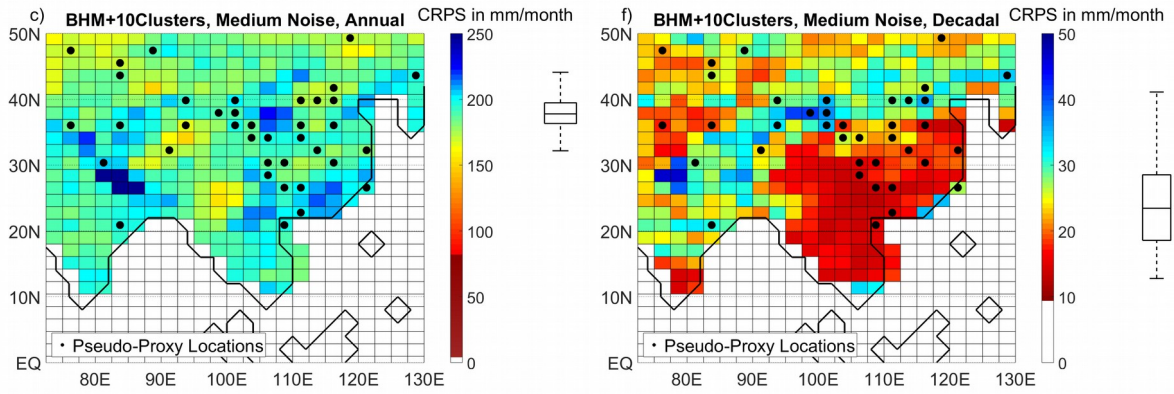
1



2



3



4

5

6

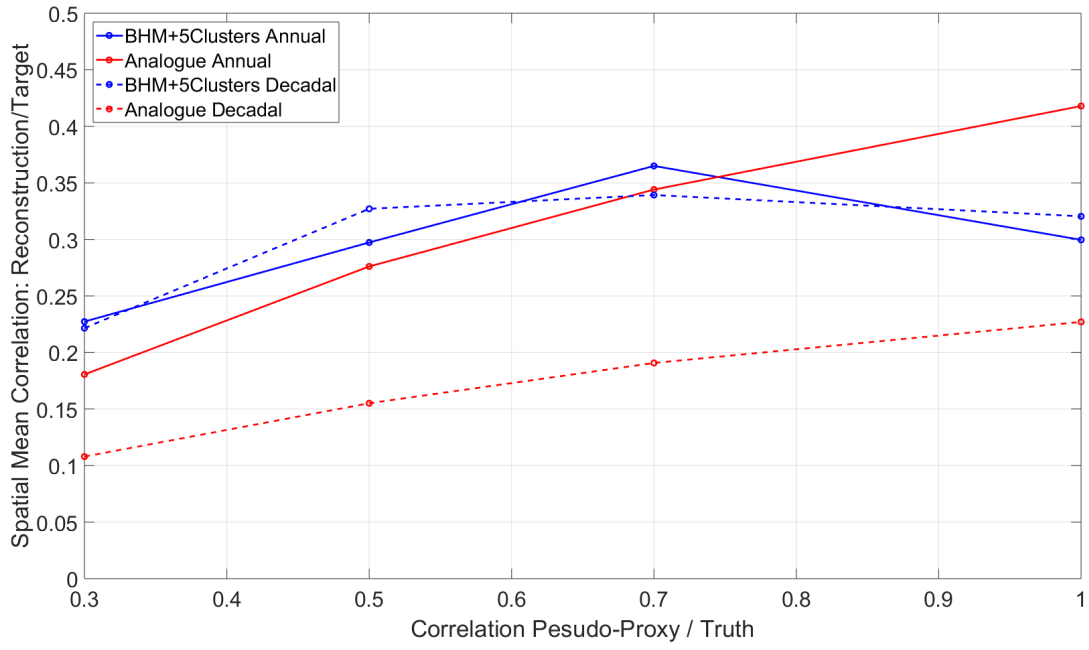
7

8

9

10

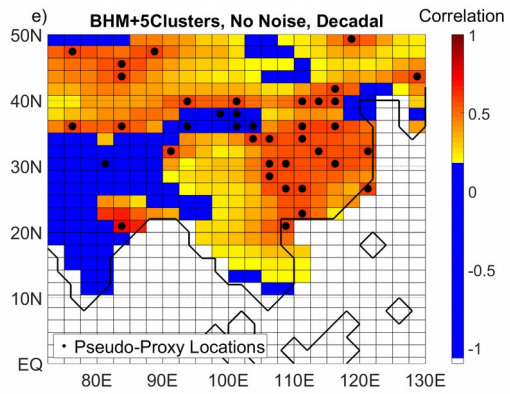
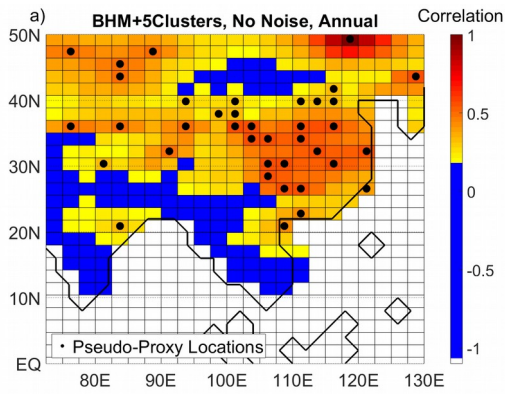
Figure 6: CRPS for different Reconstructions, at each grid point. Left: Annually-resolved data. Right: Decadally-resolved data. a) and d): BHM Reconstruction. b) and e): BHM+5Clusters. c) and f): BHM + 10 Clusters. The boxplots (indicating median, 25% and 75% percentiles and non-outlier limits) to the right of the colour bars show the distribution of the grid point CRPS. Black dots: Pseudo-Proxy network.



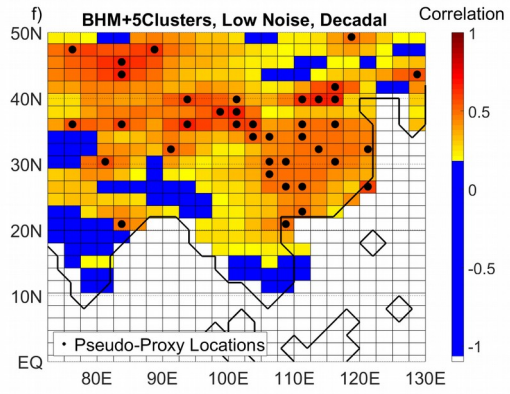
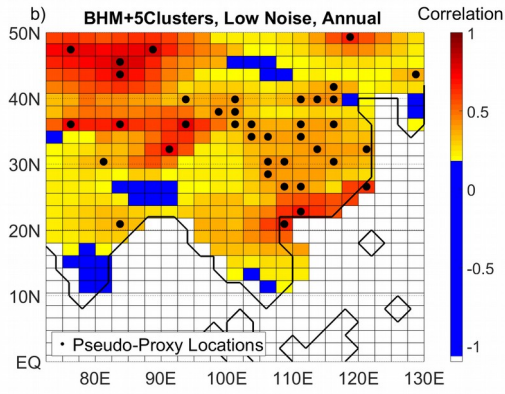
1

2 **Figure 7: Spatial Mean Correlation Skill of Reconstruction techniques for different noise**
 3 **levels (expressed here in terms of the correlation between the pseudo-proxy and truth).**

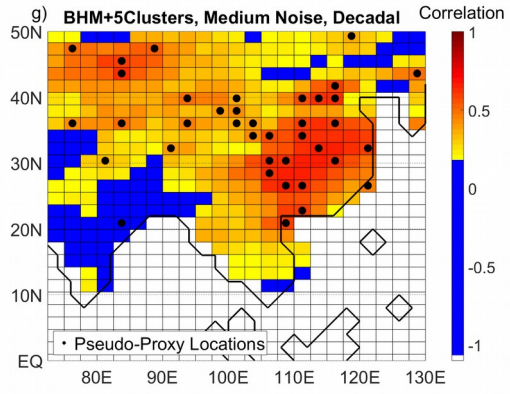
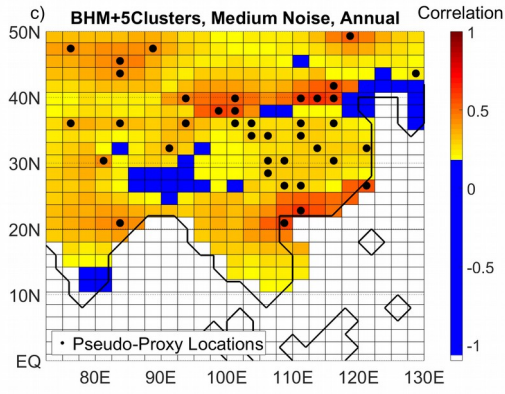
1



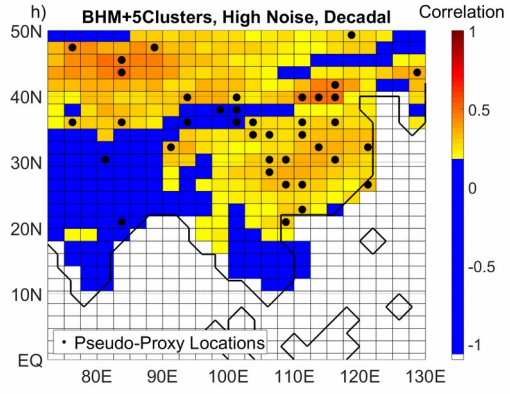
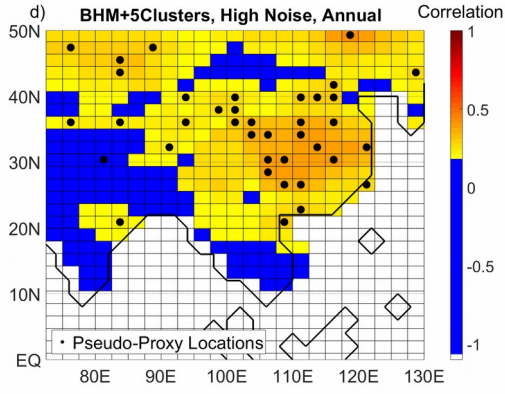
2



3



4

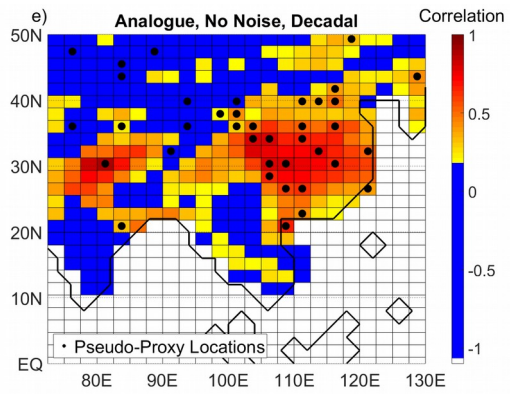
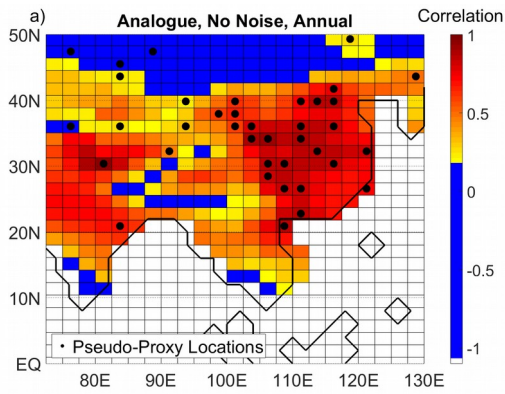


5 **Figure 8: BHM+5Clusters performance in terms of Correlation with target for different levels**
 6 **of noise at annual (left column) or decadal (right column) resolution. A and b) No noise. C and**
 7 **d) low noise. E and f) Medium-level noise. G and h) High noise.**

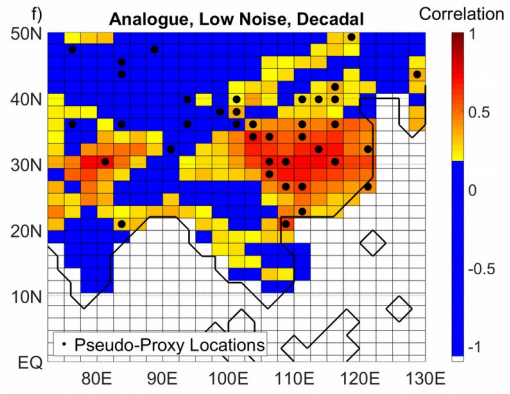
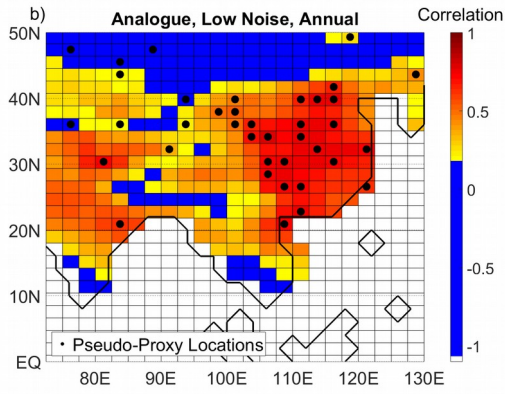
8 **The boxplots (indicating median, 25% and 75% percentiles and non-outlier limits) to the**
 9 **right of the colour bars show the distribution of the grid point Correlation Coefficients.**

10 **Black dots: Pseudo-Proxy network.**

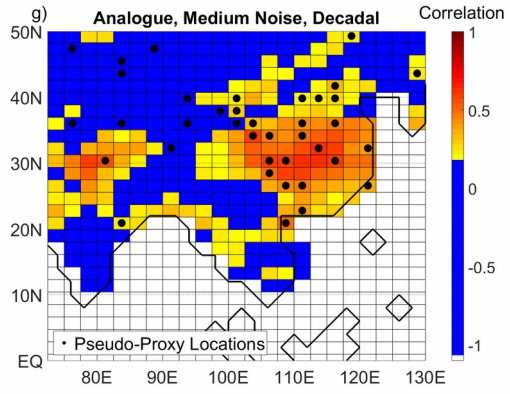
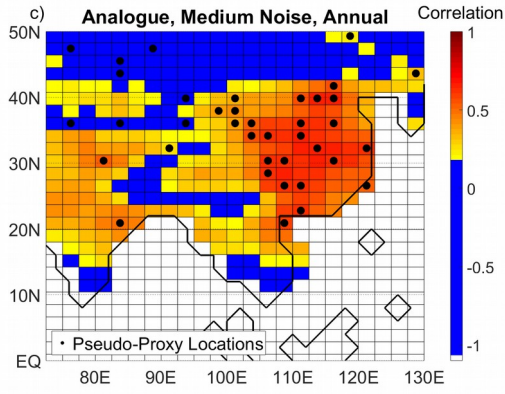
1



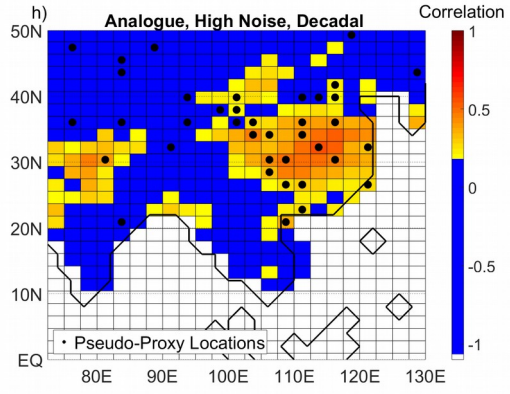
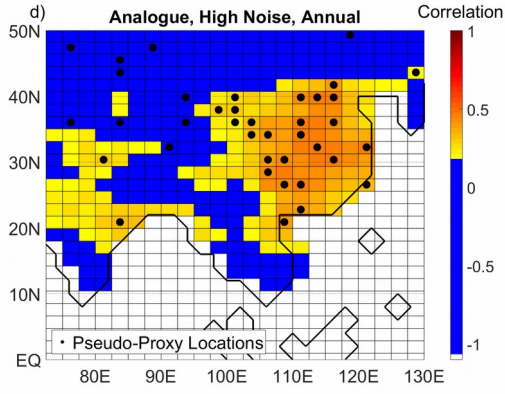
2



3



4



5

Figure 9: Analogue Method performance in terms of Correlation with target for different levels of noise at annual (left column) or decadal (right column) resolution. A and b) No noise. C and d) low noise. E and f) Medium-level noise. G and h) High noise.

6

7

The boxplots (indicating median, 25% and 75% percentiles and non-outlier limits) to the right of the colour bars show the distribution of the grid point Correlation Coefficients.

8

Black dots: Pseudo-Proxy network.

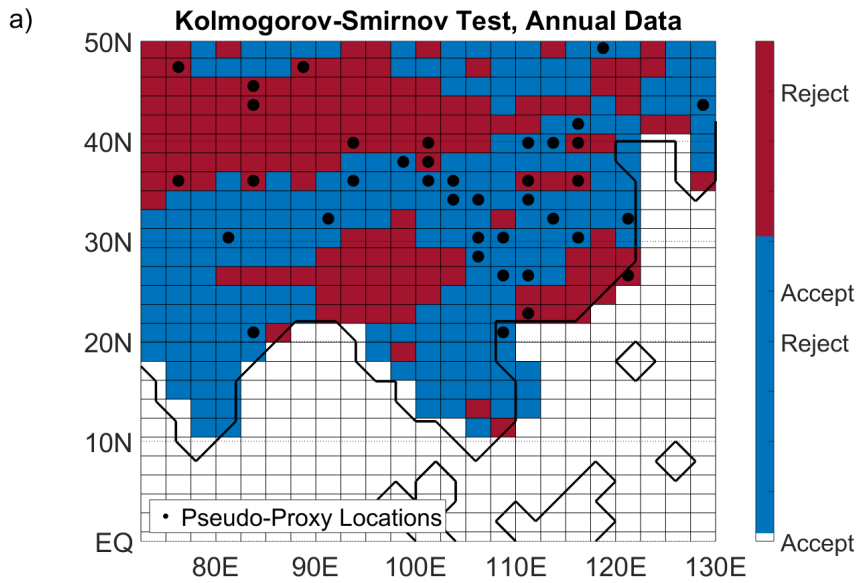
9

10

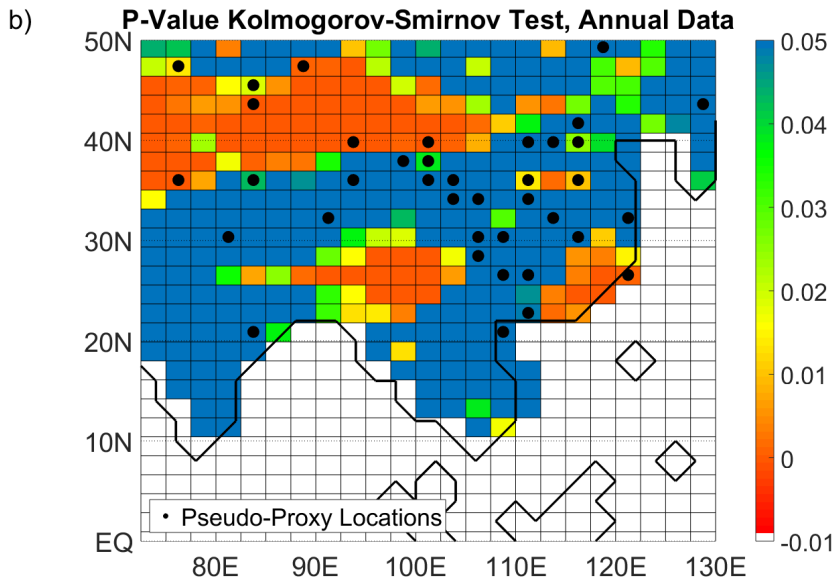
1 **Appendix A**

2
3

4



5



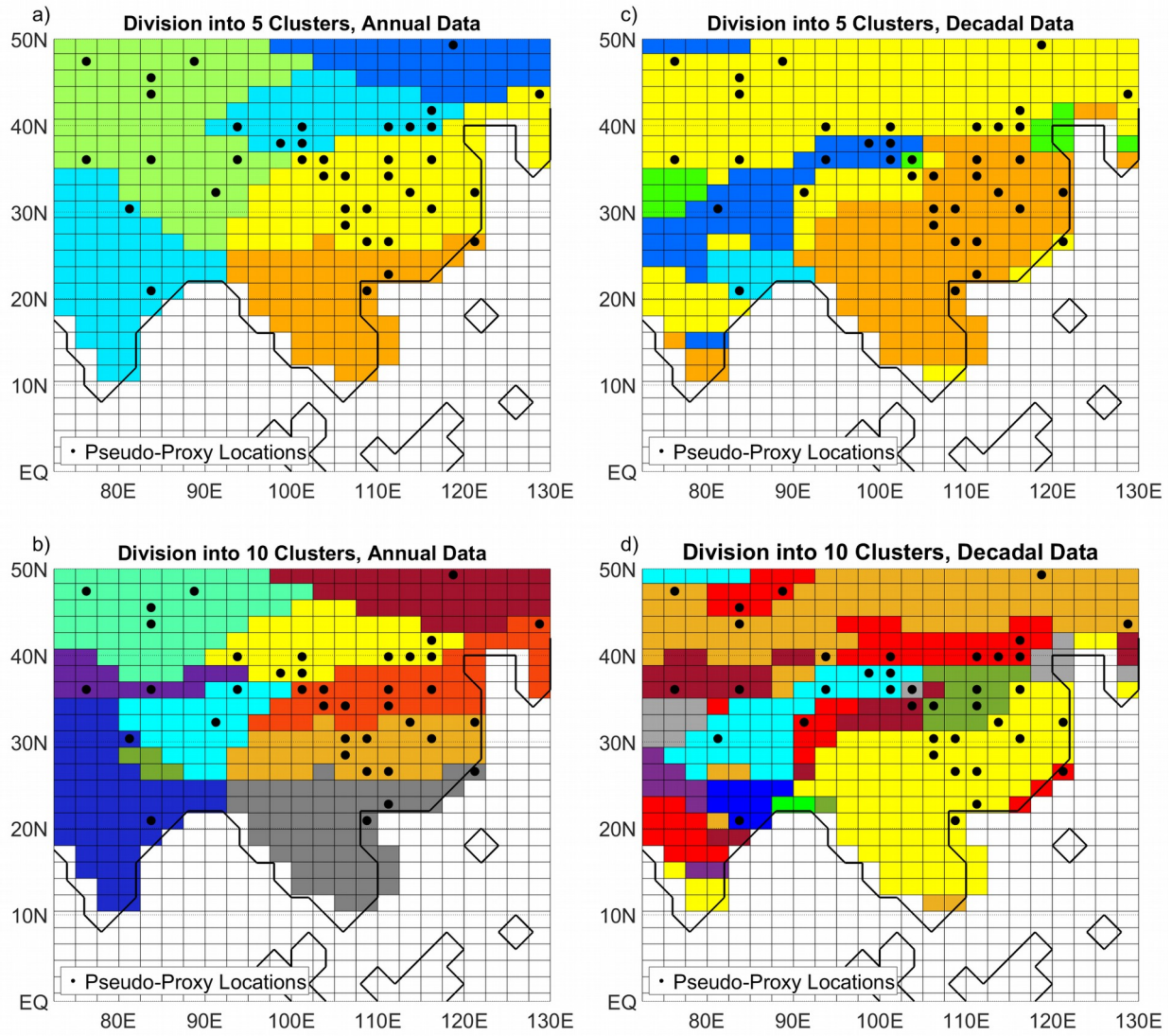
6

7 **Figure A1: Kolmogorov-Smirnov Normality test on the Simulated JJA Precipitation during**
8 **instrumental period (years 1906-2005, at annual resolution). a) Rejection or acceptance Blue:**
9 **The Normality hypothesis is rejected, White: the Normality hypothesis is not be rejected, at**
10 **a 95% confidence level, b) p-values.-**
11 **BlackMagenta dots: Pseudo-Proxy network.**

1

2

3



4 **Figure A2: Divisions into Clusters (in each plot different colors indicate different Clusters),**
 5 **using the simulated JJA precipitation in the instrumental period (years 1996-2005) as input. a)**
 6 **Annual Data, division into 5 Clusters, b) Annual Data, division into 10 Clusters, c) Decadal**
 7 **Data, division into 5 Clusters, d) Decadal Data, division into 10 Clusters. Magenta dots:**
 8 **Pseudo-Proxy network.**